Title

Ubiquitin-specific protease 8 controls B cell proteostasis and cell survival in multiple myeloma

Authors:

Almut Dufner[1,*], Fabien Thery[2,3], Gianni Monaco[1], Jelena Lazarevic[5], Oliver Gorka[1], Nina Chevalier[6], Maximilian Frosch[1], Gerbrand J. van der Heden van Noort[7], Kira Allmeroth[8], Marco Prinz[1,9,10], Olaf Groß[1,9,10], Huib Ovaa[7,†], Paul P. Geurink[7], Wolfgang W. Schamel[9,11,12], Vigo Heissmeyer[13,14], Martin S. Denzel[8,15,16], Heiko Bruns[17], Mirle Schemionek[5], Francis Impens[2,3,4], and Klaus-Peter Knobeloch[1,9*]

Affiliations:

[1]Institute of Neuropathology, Faculty of Medicine, University of Freiburg, 79106 Freiburg, Germany

[2]VIB-UGent Center for Medical Biotechnology, 9052 Gent, Belgium

[3]Department of Biomolecular Medicine, 9052 Gent, Belgium

[4]VIB Proteomics Core, 9052 Gent, Belgium

[5]Department of Hematology, Oncology, Hemostaseology and Stem Cell Transplantation University Hospital RWTH Aachen, Germany

[6] Department of Rheumatology and Clinical Immunology, Medical Center - University of Freiburg, Faculty of Medicine, University of Freiburg, 79106 Freiburg, Germany

[7]Department of Cell and Chemical Biology, Leiden University Medical Center, Einthovenweg 20, 2333 ZC Leiden, The Netherlands

[8]Max Planck Institute for Biology of Ageing, 50931 Cologne, Germany

[9]Signalling Research Centres BIOSS and CIBSS, University of Freiburg, 79106 Freiburg, Germany

[10]Center for Basics in NeuroModulation (NeuroModulBasics), Faculty of Medicine, University of Freiburg, 79106 Freiburg, Germany

[11]Faculty of Biology, Albert-Ludwigs-University of Freiburg, 79104 Freiburg, Germany

[12]Center of Chronic Immunodeficiency CCI, University Clinics and Medical Faculty, 79110 Freiburg, Germany

[13]Institute for Immunology, Biomedical Center, Ludwig-Maximilians-Universität München, 82152 Planegg-Martinsried, Germany

[14]Research Unit Molecular Immune Regulation, Helmholtz Zentrum München, 81377 Munich, Germany

[15]CECAD - Cluster of Excellence, University of Cologne, 50931 Cologne, Germany

[16]Center for Molecular Medicine Cologne (CMMC), University of Cologne, 50931 Cologne, Germany.

[17]Department of Internal Medicine 5, Hematology and Oncology, Friedrich Alexander University Erlangen-Nuremberg (FAU) and Universitätsklinikum Erlangen, Erlangen, Germany.

[†]In memory of Huib Ovaa for his seminal contributions to the ubiquitin field.

[*]Correspondence: klaus-peter.knobeloch@uniklinik-freiburg.de or almut.dufner@uniklinik-freiburg.de

Abstract

Ubiquitin-specific protease 8 exerts multiple cellular functions and was identified as a potential target in a multiple myeloma vulnerability screen. Here we characterized the function of USP8 in B cells and multiple myeloma, and analyzed its impact on the global and ubiquitin-modified proteome.

Usp8 deletion in mice starting at the the pre-B cell stage caused a partial block in B cell development favoring immature and innate-like B cells, as well as germinal center and plasma cells. This was accompanied by elevated immune-responses and Roquin depletion. Accordingly, correlation analyses in multiple myeloma patients revealed that low USP8 expression at diagnosis correlates with decreased survival. B cells expressing catalytically inactive USP8 accumulate protein modified with mixed ubiquitin/NEDD8 chains as hallmarks of proteotoxic stress, which we identified as favored USP8 substrates. USP8 knockdown reduced survival of bortezomib-resistant multiple myeloma cells in a lysosomal dysfunction-dependent manner. In contrast, the inhibitor DUB-IN-2 resensitized bortezomib-resistant multiple myeloma cells to treatment in a bortezomib-synergistic manner. Hence, our analyses uncovered the therapeutic potential of USP8 inhibition and of DUB-IN-2 in multiple myeloma.

Key words: Ubiquitin-specific protease 8/ B cells/ multiple myeloma/ proteotoxic stress/ NEDD8

Introduction

Ubiquitin modification represents a highly versatile mechanism to control cellular functions. Targeting the ubiquitin proteasome system (UPS) has been shown to represent an effective strategy for the treatment of B-cell malignancies such as multiple myeloma (MM) [1]. However, although proteasome inhibition by bortezomib (BTZ, Velcade®) has greatly enhanced patient outcome, relapse is common in MM and limits therapeutic efficacy. As a reversible process, ubiquitination is counteracted by the activity of ubiquitin deconjugating enzymes (DUBs) [2]. More than 90 different DUBs including around 50 members of the ubiquitin specific protease (USPs) family exist. USP8 represents such a USP and is characterized by a multi-domain architecture essential for various cellular functions [3]. Interactions with components of endosomal sorting complexes required for transport (ESCRT), such as STAM2 and charged multivesicular body (CHMP) proteins, have established the regulation of endosomal sorting and the control of transmembrane protein stability as canonical USP8 functions [3]. The C-terminal part of USP8 harbors the catalytic domain, which is inhibited by phosphorylation-dependent 14-3-3 binding to the N-terminus [4,5]. Somatic mutations in the exon encoding the 14-3-3 binding motif of USP8 are associated with Cushing's disease (CD) leading to the stabilization of the EGFR in ACTH-secreting pituitary adenomas [6,7]. USP8 was also associated with autophagy and mitophagy regulation [3,8,9], and has been implicated in the progression of many cancer types including effects on the tumor microenvironment via regulation of PD-L1 and regulation of TGF-β signaling and inflammatory responses [10–13].

The ubiquitin-like (ubl) modifier with the highest similarity to ubiquitin is NEDD8 [14]. Similar to ubiquitin conjugation, NEDDylation is a sequential process brought about by the NEDD8 activating enzyme (NAE), a heterodimer of NAE1 and UBA3, the conjugating enzymes UBE2M (UBC12) and UBE2F, and a set of E3 ligases. The best-established NEDDylation targets are cullin

proteins, which stimulate cullin-RING E3 ubiquitin ligases (CRLs) upon mono-NEDDylation. In contrast to canonical NEDDylation, overexpression of NEDD8 or proteasome inhibition leads to a shift in the free ubiquitin-to-NEDD8 ratio which ultimately triggers atypical conjugation of NEDD8 by the ubiquitin activating enzyme E1 (UBE1/UBA1) and the E3 ligase HUWE1 leading to the formation of mixed ubiquitin/NEDD8 chains [15–20]. These hybrid ubiquitin/NEDD8 chains represent a physiologically highly relevant defense mechanism against proteotoxic stress [20,21].

In T cells, USP8 is essential for the positive selection of thymocytes [22]. Mice with a T-cell-specific deletion of USP8 have a defect in homeostatic and antigen-driven T cell expansion. They spontaneously develop colitis concomitant with dysfunctional regulatory T cells, a phenotype that may be caused in part by a defect in USP8-mediated CTLA-4 deubiquitination [23]. Moreover, USP8 interacts with GRB2-related adaptor protein downstream of Shc (GADS) and controls stability of the ESCRT component CHMP5, which was shown to stabilizes the anti-apoptotic Bcl2 protein via direct interaction as a prerequisite for positive selection of thymocytes [22,24].

Ubiquitination and deubiquitination are also important processes in the regulation of B cell activation, proliferation, and apoptosis during development and their functional diversification and activation in innate and humoral immune responses [25]. A systems-wide analysis of B cell receptor signalosomes has identified USP8 as an interacting component upon stimulation [26]. Interest in the function of USP8 in B cells is further fueled by an RNA interference lethality screen, which uncovered *Usp8* as one of the most striking differential functional vulnerability genes between MM and non-MM cells [27]. MM cells, which represent cancerous plasma cells, are engaged in rapid protein synthesis, strongly depend on ubiquitin proteasome system (UPS)-mediated protein turnover, and are highly susceptible to perturbations of protein homeostasis. However, the precise role of USP8 in B cell function, development, and MM remains elusive.

Here we have comprehensively analyzed mice with deletion of *Usp8* at different stages of B cell-development. *Usp8*$^{f/f}$*Cd19*-Cre B mice are characterized by a predominance of immature and innate-like B cells, and germinal center (GCs) and plasma cells (PCs) with elevated immune-responsive functions. Shotgun, ubiquitinome and signal transduction analyses of B and MM cells with manipulated USP8 activity uncovered a fundamental role of USP8 in preventing proteotoxic stress-induced cell death. Of note, USP8 directly controls branched NEDD8/ubiquitin conjugation typically associated with proteotoxic stress. However, while the inhibitor DUB-IN-2, which was published to target USP8 [28], resensitized BTZ resistant MM cells to treatment in a BTZ-synergistic manner, USP8 knockdown had a BTZ-independent effect on cell survival, which was related to lysosomal dysfunction. Thus, both the use of DUB-IN-2 and specific targeting of USP8 represent promising strategies to treat B cell malignancies that are resistant to proteasome inhibition.

Results

USP8 is essential for B cell development

We have shown that USP8 is critical for T cell homeostasis where GADS has been identified as a USP8 binding partner [22]. However, B lymphocytes express only marginal levels of GADS (Fig. S1A). To evaluate the roles of USP8 in B cells, we generated *Usp8*$^{f/f}$*Cd19*-Cre mice, which delete Usp8 from the pre B cell stage on, and compared them to *Usp8*$^{f/f}$ mice (Fig. S1B). Protein expression of USP8 was not completely abrogated in splenic *Usp8*$^{f/f}$*Cd19*-Cre B cells indicating that cells with incomplete Usp8 deletion benefit from a survival advantage (Fig. S1C).

In contrast to T cells, percentages and total numbers of CD19^{+} B cells are reduced in the spleens of *Usp8*$^{f/f}$C*d19*-Cre mice (Fig. 1A). *Usp8*$^{f/f}$*Cd19*-Cre mice displayed a more pronounced reduction of follicular B cells as compared to marginal zone B cells (Fig. 1B), consistent with a defect in the development of mature (IgM^{+}/IgD^{+}) B cells in the spleen (Fig. 1C). Likewise, *Usp8*$^{f/f}$*Cd19*-Cre mice exhibited a significant reduction in the percentages of CD19^{+} and IgM^{+}IgD^{+} BM B cells, but not early developmental BM B cells (Fig. 1 D). Transitional B cell development was impaired starting from the T2 stage (Fig. 1E). The developmental defects of *Usp8*$^{f/f}$*Cd19*-Cre B cells were confirmed using *Usp8*$^{+/+}$*Cd19*-Cre mice as controls (Fig. S1D). Moreover, B1a and B1b subsets tended to show lower numbers in spleen and peritoneal cavity (PC) in the absence of USP8, while percentages within the IgM^{+} subset increased (Fig. S1E). Analyses of the splenic architecture of *Usp8*$^{f/f}$*Cd19*-Cre mice confirmed the developmental defects of B cell subsets (Fig. S1F). Consistent with the severe reduction of IgM^{+}IgD^{+} B cells, the reduction in size of B cell-rich (B220^{+}) areas was primarily caused by diminishment of primary B cell follicles (FO). Moreover, USP8 knockout (KO) cells that have been stimulated by BCR or TLR4/9 engagement exhibit a defect in proliferation (Fig. S1G), and the average number of Ki67 positive cells in splenic B cell

follicles was significantly reduced in *Usp8*$^{f/f}$*Cd19*-Cre mice as compared to controls (Fig. S1H). To determine whether USP8 is critical for earlier steps in B cell development, we generated *Usp8*$^{f/f}$*mb1*-Cre mice, which delete Usp8 from the early pro B cell stage on [29]. *Usp8*$^{f/f}$*mb1*-Cre BM B cells showed a block at the pre-B cell stage as compared to *Usp8*$^{+/f}$*mb1*-Cre B controls (Fig. S1I, upper left panels). As a consequence, a complete loss of peripheral and recirculating B cells was observed (Fig. S1I).

In summary, our data demonstrate that USP8 is essential for normal B cell development at various stages.

Elevated Ig responses and robust PC numbers in *Usp8*$^{f/f}$*Cd19*-Cre mice

To more closely characterize B cell development in *Usp8*$^{f/f}$*Cd19*-Cre mice, we performed single cell RNA-seq analysis of splenic B cells enriched from *Usp8*$^{f/f}$ and *Usp8*$^{f/f}$*Cd19*-Cre mice. Unbiased clustering of the aggregated dataset produced 10 discrete clusters (Fig. S2A). Although remaining macrophages and granulocytes were overrepresented among enriched *Usp8*$^{f/f}$*Cd19*-Cre B cells, numbers of splenic *Usp8*$^{f/f}$*Cd19*-Cre monocyte/macrophage and granulocyte populations were not altered significantly (Figure S2B). B cells and PCs were extracted from individual samples and integrated to create a combined dataset allowing in-depth analyses of distinct B cell lineage populations. B cell subpopulations were annotated using top 10 (Fig. S2C) and key signature genes according to Nguyen et al. [30]. The results confirmed that *Usp8*$^{f/f}$*Cd19*-Cre follicular and transitional B cells were diminished as compared to controls (Fig. 1F). Unexpectedly, *Usp8*$^{f/f}$*Cd19*-Cre germinal center (GC)-like and PC populations were increased relative to other B cell subsets as compared to *Usp8*$^{f/f}$ controls (Fig. 1F and 1G upper panels). Total *Usp8*$^{f/f}$*Cd19*-Cre GC B cell and PC numbers were not significantly affected, including CD19^{+} PCs (Fig. 1G, lower panels). However, CD19^{+} PCs were underrepresented among *Usp8*$^{f/f}$*Cd19*-Cre PCs. Differential

gene expression analysis of MZB, FoB, PCs, and GC-like B cells revealed elevated IL-9R expression in FoB and MZB, elevated expression of specific Ig variable regions in PCs, and reduced expression of the ZFP318, a transcriptional regulator of IgD expression [31], in GC-like B cells of *Usp8*$^{f/f}$*Cd19*-Cre mice (Fig. S2D).

To study the functional capabilities of B cells *in vivo*, we measured basal serum Ig concentrations in non-immunized *Usp8*$^{f/f}$*Cd19*-Cre mice by ELISA. The levels of all Igs tested did not differ significantly between genotypes (Fig. 2A). Likewise, GC formation was not affected in spleens of TNP-KLH-immunized *Usp8*$^{f/f}$*Cd19*-Cre mice. Despite a decrease in total GC B cell numbers, percentages among B cells were not significantly affected (Fig. 2B). We also measured IgM, $IgG_{1,}$ or IgG_3 responses to defined T cell-dependent and T cell-independent immune responses (Fig. 2C). *Usp8*$^{f/f}$*Cd19*-Cre mice produced significantly elevated levels of IgM and $IgG_{3,}$ consistent with the higher tolerance of B1, MZ, and PCs towards CD19-Cre mediated USP8 knockdown.

Spleens of TNP-KLH-immunized *Usp8*$^{f/f}$*Cd19*-Cre mice contained elevated numbers of PCs as compared to controls (Fig. 2D). However, as shown for unimmunized mice, percentages of $CD19^+$ PCs within the PC compartment were reduced suggesting that CD19 negative *Usp8*$^{f/f}$*Cd19*-Cre PCs have a survival advantage that is conferred in part by the loss of Cd19 promotor-driven Cre expression and Usp8 deletion. Consistent with elevated IgM responses, *Usp8*$^{f/f}$*Cd19*-Cre mice showed higher numbers of IgM-positive, but not IgG1 positive PCs per spleen (Fig. 2E). The expression of Blimp1 and IRF4, two transcription factors essential for PC generation and function [32], remained unchanged (Fig. 2F). Likewise, splenic naïve, effector memory, and regulatory T cell populations, and basal blood IL1-β, IL-6, and TNF cytokine levels were not affected in B cell specific USP8 KO mice (Fig. S2E and S2F).

Roquin proteins, including Roquin-1 and Roquin-2, are required for shaping T and B cell-dependent immune responses [33,34]. We thus hypothesized that Roquin function might be compromised in *Usp8*$^{f/f}$*Cd19*-Cre B cells. We monitored Roquin levels in splenic *Usp8*$^{f/f}$*Cd19*-Cre B cells using a Roquin1/2-specific antibody [35]. Indeed, Roquin appeared to be degraded in splenic USP8-deficient B cells as compared to *Usp8*$^{f/f}$ controls and Stam2, which has been reported to be stabilized by USP8 in other cells [36,37] (Fig. 2G). To evaluate whether USP8 directly controls Roquin stability, we ablated USP8 in *Usp8*$^{f/f}$*Rosa26*-Cre-ERT2 splenic B cells *ex vivo* by administration of 4-hydroxytamoxifen (OHT) in a timely controlled manner. Remarkably, this short-term *ex vivo* USP8 ablation did not directly affect Roquin protein levels and did not abolish CHMP5 expression (Fig. S3A). Thus, altered Roquin protein levels in *Usp8*$^{f/f}$*Cd19*-Cre B cells are rather a consequence of altered B cell composition and/or signaling than of a direct stabilizing effect mediated by USP8 deubiquitination. Roquin cleavage is mediated by Malt1 and the protease function of Malt1 is positively controlled by mono-ubiquitination at lysine 644 or excess exposure to free ubiquitin [38,39]. However, we did not observe elevated mono-ubiquitination of Malt1 in *Usp8*$^{f/f}$*Cd19*-Cre B cells (Fig. 2G). Although the precise mechanism of Roquin degradation and potential Malt1 activation upon USP8 depletion in B cells remain elusive, gene expression of Roquin and Malt1 correlate accurately with USP8 expression in different B cell subtypes (Fig. 2H) suggesting intertwined regulatory mechanisms.

In line with elevated Ig responses in *Usp8*$^{f/f}$*Cd19*-Cre mice, we observed elevated JNK activation (Fig. S3B) and Ca^{2+} mobilization (Fig. S3C) in the splenic B cell compartment of *Usp8*$^{f/f}$*Cd19*-Cre mice in response to anti-IgM-stimulation, while Erk1/2, p38, AKT, and IκB (Fig. S3B) or overall tyrosine phosphorylation (Fig. S3D) was not significantly affected. However, similar to Roquin, *ex vivo* induced depletion of USP8 in *Usp8*$^{f/f}$*Rosa26*-Cre-ERT2 splenic B cells did not significantly affect JNK (Fig. S3E) and Ca^{2+} signaling (Fig. S3F). Pathway enrichment

analysis of different B cell subsets revealed upregulated BCR second messenger signaling and Rho-GTPase signaling in USP8 deficient FoB cells, as well as upregulated Rho GTPase and death receptor (DR)/TNFR signaling in GC-like USP8 deficient B cells. Control FoB cells differ from USP8 KO FoB cells by altered expression of genes mainly involved in (mitochondrial) translation, RNA processing, and responses to cellular stress. USP8 deficient MZB cells are most affected with regard to ER Golgi anterograde transport and p53 signaling. In addition, Raf and CD28 signaling is enhanced. In contrast, USP8-deficient PCs vary from control PCs primarily with regard to processing of capped intron-containing mRNA. Of note, also NEDDylation, stress response, RUNX3 regulation and UCH proteinase pathways were found to be upregulated (Fig. S3G).

In summary, PCs, GC-like B cells, immature, and innate-like B cells dominate the splenic B cell compartment of *Usp8*$^{f/f}$*Cd19*-Cre mice. USP8 deficient B cells mediate increased Ig, Ca^{2+} and JNK responses, which may be a consequence of altered Rho-GTPase signaling and Roquin depletion.

USP8 limits proteotoxic stress and cleaves ubiquitin/NEDD8 mixed chains

To further address the molecular mechanisms of USP8 function in B cells, we stably expressed FLAG-tagged mouse wild type (WT)-USP8 and catalytically inactive mouse USP8(C748A) in the murine K46Lµm B cell line (Fig. 3A) and analyzed the proteome and its modification by ubiquitin and ubiquitin-like modifiers using the diGly enrichment method (Ubiscan®) [40]. Overexpression of catalytically inactive variants of USPs is a suitable approach to trap USP substrates [41]. Surprisingly, NEDD8 levels were elevated in B cells expressing catalytically inactive USP8 (Fig. 3B, left panel), and multiple ubiquitin/ubl modified sites on NEDD8, including K11, K22, K33, K48, K54, and K60, were identified (deposited in PRIDE database, identifier PXD024395; for database accession details please see methods section). These

data indicated that free or conjugated NEDD8 levels were increased in the presence of catalytically inactive USP8 and that NEDD8 itself is modified by ubiquitylation or NEDDylation, which cannot be distinguished by the diGly enrichment method. Moreover, enhanced ubiquitin/ubl-modification of specific sites of the ribosomal proteins Rpl7, Rpl8, Rpl11, and ribosome biogenesis regulator 1 (Rrs1) as well as the regulatory 26S proteasome subunit Psmd2 were detected in the presence of catalytically inactive USP8 (Fig. 3B, right panel). Ribosomal substrates typically form nuclear aggregates upon modification by ubiquitin/NEDD8 mixed chains to protect the nuclear UPS from an increased load of substrate proteins and represent a classic hallmark of proteotoxic stress [20]. In accordance with a role of USP8 in the control of NEDDylation, overall NEDDylation was strongly enhanced if we co-expressed HA-tagged NEDD8 with human FLAG-tagged catalytically inactive USP8(C786A) in HEK293T cells as compared to coexpression with WT USP8 (Fig. 3C). To examine whether these ubl modifications were comprised of NEDD8 and ubiquitin, we performed HA-NEDD8 pulldowns. Indeed, ubiquitinated proteins were present in the HA-NEDD8 pulldown of protein lysates from cells expressing USP8(C786A)-FLAG, strongly suggesting the presence of mixed chains (Fig 3D). Vice versa, FLAG-USP8(C786A) pulldowns comprised NEDDylated proteins, but not free NEDD8, indicating that catalytically inactive USP8 traps NEDDylated substrates possibly via ubiquitin incorporated into mixed ubiquitin/NEDD8 chains (Fig 3D). Likewise, mass spectrometry (MS) protein quantification of the HA-NEDD8 pulldowns showed enhanced accumulation of catalytically inactive USP8 as compared to the HA-NEDD8 pulldown performed with cells expressing WT-USP8-FLAG (Fig. 3E). Moreover, UBE1 (UBA1), HUWE1, UBA52 (ubiquitin), and DNAJB2 (HSJ1), a heat shock protein [42,43], were significantly enriched in the HA-NEDD8 pulldowns performed with cells expressing USP8(C786A)-FLAG. UBE1 and HUWE1 represent the characteristic E1 and E3 ligase in proteotoxic stress-induced non-canonical NEDDylation, respectively [15–18,20]. Quantification of K-ε-GG modified peptides uncovered the

enrichment of K11- and K48-linked ubiquitin/ubl-modifications of NEDD8 and ubiquitin in the same pulldown sample, suggesting that chains containing NEDD8 and/or ubiquitin are formed primarily via K11 and K48 linkages (Fig. 3E). Indeed, when we converted the modified HA-NEDD8 lysine (K) residues K11 and K48 to arginine (R), a significant decrease in ubiquitination and NEDDylation was observed (Fig. S4). Moreover, NEDD8 (K22 and K33) and ubiquitin (K63) modifications were present solely in the HA-NEDD8 pulldowns performed with HEK293T cells expressing catalytically inactive USP8(C786A)-FLAG (deposited in PRIDE database, identifier PXD024755). In agreement with non-canonical NEDDylation, the NAE1 inhibitor MLN4924 inhibited Cullin neddylation, but not NEDDylation caused by overexpression of catalytically inactive USP8 (Fig. 3F). In line with previous data showing that USP8 does not catalyze deNEDDylation [44], USP8 formed a covalent linkage solely with a ubiquitin-propargylamide (PRG) probe [45,46], but not with NEDD8-PRG, which exclusively targeted the deNEDDylating enzyme Sentrin-specific protease 8 (SENP8) [47] (Fig. 3G).

The identification of NEDD8-modified substrates besides cullins has been hampered by the lack of efficient MS approaches that can distinguish between ubiquitin and NEDD8 modifications [48]. To confirm ubiquitin/NEDD8 hybrid chain formation, we co-expressed catalytically inactive USP8 (and WT USP8) with HA-tagged WT NEDD8 and a variant of NEDD8, in which the C-terminal LRGG sequence was changed to LTGG. This variant of NEDD8 is still linked to substrates (Fig. 3H, left panels), but trypsin cannot generate the K-ε-GG remnants on which MS identification of the ubiquitin/ubl modification sites is based [49]. Following HA-pull down, MS analysis revealed that both WT-NEDD8(LRGG) and NEDD8(LTGG) were modified on K48, indicating that NEDD8(K48) represents an ubiquitination site (Fig. 3H, right panel). Vice versa, modification of ubiquitin at K63 was detected in the presence of exogenously expressed NEDD8(LRGG), but not NEDD8(LTGG), indicating that ubiquitin is NEDDylated at K63. While our data do not exclude

that K48 on both NEDD8 and ubiquitin can further be modified by NEDD8, they clearly confirm the presence of mixed ubiquitin/NEDD8 chains. In line with USP8-mediated cleavage of ubiquitin in ubiquitin/NEDD8 mixed chains, modification of substrates was diminished by recombinant USP8 (Fig. 3I). Strikingly, DUB cleavage assays performed *in vitro* with recombinant USP8 and synthetic K48-ubiquitinated NEDD8 or K48-diubiquitin verified that USP8 indeed cleaves ubiquitin/NEDD8 branches more efficiently than K48-diUb (Fig. 3J).

These data confirm the formation of mixed ubiquitin/NEDD8 chains as hallmarks of proteotoxic stress in the presence of catalytically inactive USP8 and the direct involvement of USP8 in the negative control of these heterotypic chains.

USP8 controls proteostasis and survival in MM

Our data suggested that exogenously expressed catalytically inactive USP8 induces proteotoxic stress. Thus, we monitored the functional consequences of OHT-induced USP8 deletion in primary *Usp8*$^{f/f}$*Rosa26*-CreERT2 B cells. In these cells, the formation of ubiquitin linkages was increased 72 h post OHT addition as compared to controls (Fig. 4A). USP8 ablation did not affect Stam2 and 14-3-3 protein expression or substrate NEDDylation, but a trend to accelerated apoptosis (Fig. 4A, right panels) correlated with slight increases in Caspase 3, Caspase 8 and JNK activation (Fig. 4B).

Induction of hyperNEDDylation in USP8-depleted primary B cells may require increased, free NEDD8 levels. However, additional MLN4924 treatment of USP8-depleted cells inhibited Cullin NEDDylation and increased free NEDD8 levels, but did not cause significant hyperNEDDylation (Fig. 4C). These data suggest that cell type-specific redundant pathways are capable of removing mixed NEDD8 chains from substrates. The presence of catalytically inactive USP8 may be required to stabilize mixed ubiquitin/NEDD8 chains.

In primary B cells, USP8 depletion leads to an increase in autophagy shown by an increase in the lipidated form of LC3 (Fig. 4C). However, ER stress typically leading to an increase in the expression of the transcription factors CHOP and XBP1s upon engagement of the master regulator BiP/GRP78 and its downstream effectors PERK, IRE1, and ATF6[50] is only induced if UBA1-mediated ubiquitination is inhibited by MLN7243 (Fig. 4C). Interestingly, UBA1 inhibition leads to USP8 cleavage which correlates with strong caspase 3 activation (Fig. 4C).

In summary, these results reveal cell type and/or manipulation type specific consequences of USP8 inhibition all leading to increases in overall ubiquitination and proteotoxic stress.

Usp8 has been identified as a vulnerability gene in MM, a disease characterized by clonal expansion of malignant PCs in the bone marrow, which are highly susceptible to disturbed protein homeostasis [1,27]. Thus, we speculated that inhibition of USP8 catalysis can enhance proteotoxic stress ultimately resensitizing proteasome inhibition resistant malignant MM cells. To investigate whether inhibition of USP8 can overcome BTZ resistance, we exposed KMS-18 and KMS27 MM cells or BTZ resistant variants thereof (expressing the proteasomal subunit PSMB5 harboring a T21A or an A49V substitution in the BTZ binding pocket, respectively [51]) to BTZ. In addition we applied the inhibitor DUB-IN-2, which has been reported to target USP8 [28], or a combination of BTZ and DUB-IN-2. Indeed, while neither BTZ nor DUB-IN-2 sufficiently affected KMS-18-T21A or KMS-27-A49V viability, a combination of both drugs severely reduced cell viability (Fig. 4D) and caused excessive accumulation of polyubiquitylated proteins already after 6 h (Fig. 4E and 4F). To overcome BTZ resistance of KMS-18-T21A cells a DUB-IN-2 concentration of 25 µM was required (Fig. S5). As shown for UBA1 inhibition in primary B cells, exposure to BTZ led to USP8 protein degradation and caspase 3 activation in the KMS-18 WT cell line after 24 h of treatment, which was severely enhanced by co-treatment with DUB-IN-2. In KMS-18-T21A cells, caspase 3 was activated exclusively upon combined BTZ/DUB-IN-2 treatment (Fig. 4E, right

panels). Similar patterns were seen with regard to upregulation of CHOP and its target death receptor 5 (DR5). CHOP was upregulated already 6 hours after DUB-IN-2 treatment, with BTZ/DUB-IN-2 co-treatment being most effective (Fig. 4E, left panels). Unexpectedly, XBP1s expression did not parallel upregulation of CHOP in the presence of DUB-IN-2. XBP1s expression may therefore be cell type dependent and under tight control in MM cells to promote pro-apoptotic functions as opposed to pro-adaptive functions [52,53]. Autophagy was not affected as the lipidated form of LC3 did not accumulate upon inhibitor treatment under all conditions (Fig. 4E). Similar patterns of CHOP, XBP1s, and LC3 regulation upon 6 h inhibitor treatment were found in KMS-27 MM cells and the KMS27-A49V derivative (Fig. 4F).

In summary our findings indicate that DUB-IN-2 can be used therapeutically to overcome BTZ resistance by means of increasing ER stress responses.

DUB-IN-2 exerts USP8 inhibition-independent effects on cell viability

To assess whether the consequences of USP8 depletion in MM cells parallel the effects seen with DUB-IN-2 treatment, we depleted USP8 in KMS cell variants with siRNA followed by treatment with BTZ. In contrast to combined BTZ/DUB-IN-2 treatment, combined USP8 depletion and BTZ treatment had an additive rather than a synergistic effect on cell viability of KMS-18-T21A and KMS-27-A49V cells, with KMS-27-A49V cell being more susceptible (Fig. 5A). This effect required 3x higher BTZ concentrations than the synergistic effect observed with BTZ/DUB-IN-2 co-treatment. In contrast to DUB-IN-2 treatment, USP8 depletion did not induce CHOP or enhance CHOP induction by BTZ, but had profound effects on Caspase 8 and Caspase 3 activation (Fig. 5B). These results suggested that DUB-IN-2 may affect BTZ-resistant MM cell viability independently of USP8 inhibition.

To further assess DUB-IN-2 specificity, we depleted USP8 in these cells using pooled or 2 individual siRNAs directed against USP8 followed by BTZ, DUB-IN-2, or BTZ/DUB-IN-2 treatment (Fig. 5C). USP8 was depleted efficiently with pooled siRNA or siRNA_2, whereas siRNA_1 was less effective (Fig. 5D). Again, USP8 depletion and BTZ additively reduced cell viability, which was further decreased by additional DUB-IN-2 treatment (Fig. 5C). Strikingly, although USP8 depletion did not increase CHOP expression, its transcriptional target DR5 was strongly upregulated and correlated with caspase 8 activation. In contrast, 6h DUB-IN-2 and/or BTZ treatment had no effect on DR5 expression or caspase activation (Fig. 5D). To exclude potential USP8 siRNA off-target effects, we rescued USP8 expression upon USP8 siRNA_2 depletion in 293T cells. Both exogenous WT USP8 and USP8 harboring a silent mutation in the siRNA_2 target sequence rescued USP8 depletion-induced hyper-ubiquitylation, DR5 upregulation - and JNK activation - which has previously been shown to act upstream of DR5 transcriptional activation [54] (Fig. 5E). Thus, JNK activation may represent a CHOP-independent pathway of DR5 induction in response to USP8 depletion. Indeed, siRNA-mediated depletion of CHOP in KMS18-T21A cells confirmed that DR5 is induced by USP8 knockdown in a CHOP-independent manner (Fig. 5F). Moreover, CHOP was not required for cell death induced by combined BTZ/DUB-IN-2 treatment (Fig. 5F and 5G). In agreement with USP8 depletion-induced JNK activation, which induces apoptosis via extrinsic and intrinsic pathways [55], caspase 3, 9, and 8 were activated upon USP8 depletion (Fig. 5 F).

Differential effects of USP8 depletion or DUB-IN-2 activation on downstream pathways may be the consequence of differential regulation of protein degradation. Because USP8 is implicated in lysosomal trafficking and degradation of transmembrane proteins [3], we stained lysosomes of KMS-18-T21A cells, that have been either depleted of USP8 with siRNA or treated with BTZ and/or DUB-IN-2, with acridine orange (AO). Exclusively upon USP8 depletion lysosomes were

enlarged indicating dysfunctional lysosomal protein degradation (Fig. 5H). We next treated KMS-18-T21A cells with folimycin to induce lysosomal dysfunction. In agreement with the downstream effects seen with USP8 depletion, folimycin strongly induced JNK and DR5 expression with little effects on CHOP expression. Moreover, overall protein ubiquitylation was enhanced only 24 h post folimycin addition (Fig. 5I). These results indicate that DUB-IN-2 targets largely USP8-independent proteasomal degradation, which might also explain the synergistic effect seen with BTZ inhibition.

To rule out the possibility that DUB-IN-2 inhibits autophagosomal protein degradation, we treated KMS-18-T21A cells with bafilomycin in the presence or absence of DUB-IN-2, BTZ or both inhibitors. Bafilomycin inhibits autophagosomal/lysosomal fusion allowing stabilization of the lipidated form of LC3, which was not altered upon inhibitor treatment. In agreement with the pro-apoptotic function of IRE1 in ER stress [52,53], JNK and caspase 8 were strongly induced upon 12 h BTZ/DUB-IN-2 treatment with no effects on DR5 expression (Fig. 5J). These results indicate that apoptosis in MM cells treated with BTZ and DUB-IN-2 is mediated by (ER stress-induced) JNK activation in a DR5-independent manner, whereas USP8 depletion triggers JNK activation, DR5 upregulation, and apoptosis largely by compromising lysosomal function [56] (Fig. 5K).

To determine whether Usp8 is associated with MM in patients, we investigated the survival rate of patients from the MMRF-COMMPASS study (https://portal.gdc.cancer.gov/projects/MMRF-COMMPASS) with high (>65%), low (<35%), and mid (>35% & <65 %) Usp8 expression at time of diagnosis. Unexpectedly, the survival rate of MM patients with low USP8 expression was significantly poorer than that of patients with higher USP8 expression (Fig. 6A). Accordingly, pathway enrichment analysis uncovered upregulation of genes involved in DNA replication in patients with low Usp8 expression at time of diagnosis, whereas genes involved in translation were upregulated in patients with high Usp8 expression (Fig.

S6A). Expression of Usp8 did not differ depending on disease stage, however (Fig. 6B). Taken together, these results are in agreement with the finding that PCs are highly resilient to incomplete USP8 depletion in mice. Consequently, a distinct threshold of USP8 inhibition may be required for beneficial effects on MM progression, whereas low USP8 expression above this threshold may have MM-specific positive effects on protein homeostasis.

Because the use of the inhibitor DUB-IN-2 was more effective in overcoming BTZ resistance than Usp8 depletion, with synergistic rather than additive effects on BTZ treatment, we finally tested the efficacy of BTZ/DUB-IN-2 combination treatment in an *in vivo* transplantation model. To this end, we reconstituted NSG mice with KMS-18 or KMS-18-T21A cells followed by treatment with BTZ alone or a combination of BTZ and DUB-IN-2. Although our KMS-18 parental and mutant cell infiltration in the BM was poor within our experimental time frame (Fig. S6B), we detected stable infiltration in the spleen and here a clear trend of reduced malignant cell expansion upon combined BTZ/DUB-IN-2 treatment in KMS-18 and KMS18-T21A transplanted mice (Fig. 6C). However, toxicity of the combination treatment was observed, which may in part be attributable to our experimental setting including irradiation of immune-compromised mice (Fig. 6D). DUB-IN-2 IP injection of immunocompetent mice was previously reported to be well tolerated at a daily dose of 3 mg/kg with a break every 6 days [10].

In summary, our findings strongly suggest that both, specific inactivation of USP8 and DUB-IN-2 treatment can be exploited therapeutically to overcome BTZ resistance in MM and trigger apoptotic pathways in B cell malignancies

Discussion

Our data demonstrate that USP8 is critical for the development of B cells at early and advanced stages. If *Usp8* is deleted at later stages (such as in *Usp8*$^{f/f}$*Cd19*-Cre mice) which allow B cell

development to progress to the pre-B cell stage, immature, innate-like B cells, GC-like B cells and PCs with diminished Roquin expression become dominant, allowing normal (IgG_1) or enhanced (IgM and IgG_3) Ig production upon immunization.

Roquin proteins, including Roquin-1 and Roquin-2, are RNA binding proteins that also possess N-terminal E3 ligase activity and are required for shaping T and B cell-dependent immune responses [33,34]. Roquin-1 inhibits the stability of miRNA and RNA targets such as *Ifng* mRNA [33] and *Icos* mRNA [57] and controls mTor activity at multiple levels [58,59]. Roquin-ablation in B cells has previously been shown to cause expansion of the total B-cell population with a slight trend towards spontaneous GC activation [60]. Likewise, *Roquin*$^{san/san}$ (sanroque) mice develop spontaneous GCs and autoimmunity as a consequence of a single mutation in the *Roquin1*/*Rc3h1* gene [61]. Preventing GC formation in sanroque mice by crossing them into a background deficient for the transcriptional co-activator Obf1 did not abolish autoimmune disease, but suggested that the expanded B1 B cell population in Obf1$^{-/-}$ mice and extrafollicular PCs contributed to IgM autoantibody generation [62]. Similarly, albeit USP8 deficiency compromises B cell expansion and differentiation, it did not prevent GC formation and PC development, and immunization of *Usp8*$^{f/f}$*Cd19*-Cre mice caused enhanced IgM and IgG_3 responses. Thus, the lack of Roquin expression in splenic USP8-deficient B cells strongly suggests that the observed higher activation potential of the splenic B cell compartment at least partly depends on the lack of Roquin function. Moreover, derepression of Roquin target genes could contribute to resistance of specific B cell subsets to USP8 depletion-induced cell death. However, despite the striking coregulation of Roquin, MALT1 and USP8 (Fig. 2H), the precise mechanism leading to *in vivo* Roquin depletion in B cells in the absence of USP8 remains elusive.

Initial indication of proteotoxic-stress-induced B cell defects in the absence of USP8 function originated from our experiments performed with K46Lμm B cells expressing catalytically inactive

USP8(C748A). In this setting, endogenous USP8 can prevent cell death and allows to enrich substrates of USP8 that are modified by mixed ubiquitin/NEDD8 chains taking advantage of a USP8(C748A)–mediated "trapping" mechanism [41]. Hybrid ubiquitin/NEDD8 chains promote nuclear protein aggregation of mainly ribosomal proteins to protect the nuclear UPS from dysfunction upon proteotoxic stress [20]. NEDDylation was also shown to regulate proteotoxic stress by promoting cytosolic aggresome-like bodies coupled to the aggresome-autophagy flux [21]. Accordingly, NEDD8 protein has been identified in multiple disease-related inclusion bodies containing ubiquitin, including Lewy bodies in Parkinson's disease and neurofibrillary tangles from Alzheimer's disease patients [63,64] corroborating its potential role in antagonizing proteotoxic stress. In accordance with other studies that investigated classical and/or proteotoxic stress-induced substrate NEDDylation [18,19,48], ubiquitin(K63) NEDDylation emerges as a novel regulatory signature specific for proteotoxic stress and functional USP8 deficiency. Moreover, for the first time we identified K48 ubiquitylation of NEDD8 as a USP8 protease target.

Deregulated proteostasis is the main cause of cell death in proliferating USP8-deficient B cells leading to the observed developmental defects and accumulation of mainly ubiquitinated substrates. Using substrate trapping by catalytically inactive USP8, it becomes apparent that USP8 functions to remove mixed ubiquitin/NEDD8 chains. The survival disadvantage in the absence of USP8 is in agreement with our finding that deletion of USP8 in B cells at defined developmental stages is accompanied by an advantage of escapee cells that still express USP8. Thus, only *ex vivo* analyses of cells where deletion of the USP8 gene is induced in a tightly controlled manner is an adequate approach to uncover the primary mechanistic defects underlying the developmental defects in USP8-deficient B cells.

Using MM as a cancer model with high susceptibility to proteasome inhibition and high rates of relapse, we show that the promotion of proteotoxic stress by the inhibitor DUB-IN-2 or USP8

knockdown can be exploited for translational applications. In particular, BTZ resistant MM cells could be efficiently targeted with a combination of DUB-IN-2 and BTZ within a therapeutic window where the inhibitor had little effect on cell viability in the absence of BTZ. MM cells strongly depend on the unfolded protein response (UPR) signaling activation due to continuous overproduction of proteins [53]. Our findings indicate that both BTZ and DUB-IN-2 elicit the ER stress response by targeting the UPS as the "Achilles heel" of MM, via a pathway that is independent of USP8 downregulation.

In contrast, USP8 depletion culminates in lysosomal dysfunction and affects MM cell viability independently of BTZ treatment, which even in the absence of USP8 protein expression acts synergistically with DUB-IN-2 to kill BTZ-resistant MM cells.

In conclusion, we identified DUB-IN-2 as a potent compound to overcome BTZ resistance in MM, which acts downstream of BTZ to enhance inhibition of the UPS. Our *in vivo* testing of combined BTZ/DUB-IN-2 treatment in a mouse transplant model encourages further studies into exploitation of DUB-IN-2 or derivatives for combination therapies.

In addition, our data encourage further investigations into identification of specific USP8 inhibitors, as blocking USP8 function represents a BTZ independent route to compromise MM cell proteostasis, which relies on lysosomal dysfunction. Likewise, the critical role and prognostic correlation of USP8 activity in various human cancers [10–13] and neurodegeneration [65,66] opens up new avenues to exploit USP8 as a drug target. Yet, because USP8 strongly affects the tumor microenvironment via regulation of PD-L1 stability, TGF-β signaling, inflammatory responses and, CTLA-4 stability [10–12,23], future investigations should involve mouse models that more closely recapitulate human cancer than transplantation models. Although early embryonic lethality [36] and fundamental problems in T and B cell development ([22] and this study) in constitutive and conditional USP8 KO mouse models raised considerable safety concerns of such a strategy,

classical genetic deletion models only partially resemble pharmacological approaches. Inhibition by small molecules usually does not eliminate overall enzymatic activity and is biased towards particular cell types and/or dependent on administration routes. However, our analyses of USP8 function in mice and MM patients strongly suggest, that overcoming a specific threshold of USP8 inhibition in MM cells is crucial to generate beneficial effects in MM treatment. As the hematopoietic system is readily accessible for pharmacologic applications, diminishing USP8 activity within this compartment should represent a promising approach for anti-oncogenic and immunomodulatory therapeutics.

Acknowledgements

We'd like to thank S. Feller and S. Adoro for antibodies, Daniel J. Fernandez for technical advice, and L. Riechert, M. Leffler, M. Ditter and T. Bass for technical assistance. F.I. was supported by an Odysseus type 2 grant from the Research Foundation Flanders (FWO) (G0F8616N)), Concerted Research Action grant BOF21/GOA/033 and Starting Grant BOF/STA/202209/011 from Ghent University, and the European Research Council (ERC Consolidator Grant #101089193). F.T. was supported by a fellowship from the Research Foundation-Flanders (FWO) (12AN524N). N. C. was supported by the IMMediate Advanced Clinician Scientist-Program, Department of Medicine II, University of Freiburg Medical Center, funded by the Bundesministerium für Bildung und Forschung (BMBF, Federal Ministry of Education and Research). O. Gr. received funding through GRK 2606 (Project ID 423813989), and under Germany's Excellence Strategy, through CIBSS - EXC-2189 (Project ID 390939984). M.S. was supported in the framework of the DFG-funded Research Training Group "Tumor-targeted Drug Delivery" grant 331065168. W.W.S. is supported by the DFG under Germany's Excellence Strategy - EXC-2189 - Project ID: 390939984 and under the Excellence Initiative of the German Federal and State Governments - EXC-294, by a research

grant (Project-ID 403222702 - SFB 1381), and in part by the Ministry for Science, Research and Arts of the State of Baden-Württemberg. This work was supported by the Deutsche Forschungsgemeinschaft (DFG) grants 423813989/GRK2606, KN590/4-2 and under Germany's Excellence Strategy (CIBSS–EXC-2189–Project ID 390939984) to KPK.

Author contributions

Conceptualization, A.D. and K.P.K.; Methodology, F.I., M.F., W.W.S., H.O., P.P.G., H.B., and M.S.; Investigation, A.D., F.T., O.G., N.C., M.F., J.L., and G.J.H.N.; Formal Analysis, A.D., G.M., F.T., and F.I., M.S.; Writing – Original Draft, A.D. and K.P.K.; Funding Acquisition, K.P.K.; Resources, M.P., H.O., P.P.G., W.W.S., O.Gr., H.B., K.A., M.S.D., and V.H.; Supervision, A.D., F.I., M.S., and K.P.K..

Declaration of interests

The authors declare no competing interests.

Figure legends

Fig. 1. Defect in B cell development in *Usp8*$^{f/f}$*Cd19*-Cre mice. (A-C) Flow cytometry analysis of B cell subsets in spleen of *Usp8*$^{f/f}$ and *Usp8*$^{f/f}$*Cd19*-Cre mice. Pre-gating is indicated at the top right of the FACS plots. Percentages and numbers of B cell subsets are shown in the right panels. (D) Flow cytometry analysis of *Usp8*$^{f/f}$ and *Usp8*$^{f/f}$*Cd19*-Cre bone marrow (BM) (paired, 2-sided t-test). (E) Flow cytometry analysis of splenic transitional *Usp8*$^{f/f}$ and *Usp8*$^{f/f}$*Cd19*-Cre B cell subsets (paired, 2-sided t-test). (F) Uniform Manifold Approximation and Projection (UMAP) of B cells enriched from spleens of *Usp8*$^{f/f}$ and *Usp8*$^{f/f}$*Cd19*-Cre spleens. (G Flow cytometry analysis of splenic *Usp8*$^{f/f}$ and *Usp8*$^{f/f}$*Cd19*-Cre germinal center (GC; GL7^{hi} ,Fas^{hi}, TCR-β^{-}, B220^{+}) B cells and CD138^{hi} PCs, and CD19 expression on PCs. MZB: marginal zone B cells; FoB: follicular B cells, Pro: pro-B cells; Pre: pre-B cells; TransB, Transitional B cells; T1, T2, T3; Transitional T1, T2, T3 B cells; BM: bone marrow; PCs, plasma cells; GC-like, germinal center-like.

Fig. 2. *Usp8*$^{f/f}$*Cd19*-Cre mice exhibit enhanced PC numbers and Ig responses upon T cell-dependent and T cell-independent immunization. (A) Normal basal immunoglobulin titers in *Usp8*$^{f/f}$*Cd19*-Cre mice. (B) Control and *Usp8*$^{f/f}$*Cd19*-Cre mice were i.p. injected with 50 μg TNP-KLH precipitated in alum and GC B cells were visualized by fluorescence imaging of frozen sections and quantified by FACS analysis (GL7^{hi} ,Fas^{hi}, TCR-β^{-}, B220^{+}) at day 14 post injection. Scale bar, 100 μm. (C) Detection of TNP-specific Ig present in the serum of *Usp8*$^{f/f}$ and *Usp8*$^{f/f}$*Cd19*-Cre mice that have been i.p. injected with 50 μg TNP-KLH precipitated in alum (TD response) or with 25 μg TNP-Ficoll (TI response) by ELISA. Significant differences are indicated in a cumulative manner. (D-F) *Usp8*$^{f/f}$ and *Usp8*$^{f/f}$*Cd19*-Cre mice were treated as in (B) and spleen single cell suspensions were analyzed by FACS to determine frequencies of CD138^{hi} PCs and CD19 expression on PCs (D), frequencies of IgM^{+} and IgG1^{+} PCs (E), as well as the expression of

Blimp1 and IRF4 in PCs (F). (G) Splenic *Usp8*$^{f/f}$ and *Usp8*$^{f/f}$*Cd19*-Cre B cells were enriched and analyzed by Western blotting (WB). Results are representative of at least 5 independent experiments. (H) Gene expression of USP8, Roquin and Malt1 genes in splenic *Usp8*$^{f/f}$ and *Usp8*$^{f/f}$*Cd19*-Cre B cell subsets. Black dots represent a single cell each.

Fig. 3. USP8 regulates mixed ubiquitin/NEDD8 chain formation indicating proteotoxic stress. (A, B) NEDD8 levels and ribosomal protein modifications are elevated in B cells expressing USP8(C748A)-FLAG. (A) WT-USP8-FLAG and USP8(C748A)-FLAG expression in K46Lμm B cells analyzed by WB. (B) Volcano plots of USP8(C748A):WT-USP8 diGly proteomics experiments. Differentially expressed proteins (shotgun analysis) and regulated diGly sites (GG-modified sites analysis) were identified in proteins derived from K46Lμm B cells expressing WT USP8 or USP8(C748A) (n=3). Lysine positions of the identified diGly sites are included in parentheses. (C-E) HEK293T cells were transfected with WT-USP8-FLAG or USP8(C786A)-FLAG in the presence of HA-NEDD8. (C) Lysates were analyzed by WB. (D) Anti-HA and anti-FLAG pulldowns were analyzed by WB. (E) Anti-HA pulldowns were analyzed by MS (n=3) to quantify pulled down proteins and GlyGly-K sites. The lysine position of the identified di-glycine site is included in parentheses. (F) HEK293T cells were transfected as in C. 24 h prior to lysis cells were treated with MLN4924 (100 nM) as indicated and ysates were analyzed by WB as indicated. (G) USP8 does not directly deNEDDylate substrates. HEK293T cells were transfected with HA-SENP8, WT-USP8-FLAG or USP8(C786A)-FLAG. Lysates were incubated with buffer alone (ctr.), NEDD8-propargylamide (NEDD8-PRG), or ubiquitin-PRG and analyzed by WB using anti-HA or anti-FLAG antibodies. (H) HEK293T cells were transfected with WT-USP8-FLAG or USP8(C786A)-FLAG in the presence of HA-NEDD8(LRGG) or HA-NEDD8(LTGG). Lysates were analyzed by WB (left panels). Anti-HA pulldowns were analyzed by MS (3

replicates/condition) and alterations of ubiquitin (UBA52) and NEDD8 diGly sites are shown in the heat map. Hybrid linkages between both modifiers are reconstructed in the scheme below. (I) Protein lysates generated from 293T cells transfected with USP8(C786A)-FLAG and HA-NEDD8 were incubated with recombinant USP8 as indicated and analyzed by WB. (J) DUB cleavage assays were performed with recombinant human full length USP8 and synthetic K48-ubiquitinated-NEDD8 or K48-diubiquitin for the times indicated. The resulting cleavage products were visualized after protein electrophoresis and protein staining of the gel. Results are representative of 3 independent experiments.

Fig. 4. USP8 knockdown and BTZ/DUB-IN-2 treatment induce proteotoxic stress and apoptosis in proliferating cells with DUB-IN-2 inducing re-sensitization of resistant MM cells to BTZ. (A) *Usp8*$^{f/f}$ and *Usp8*$^{f/f}$*Rosa26*-CreERT2 splenic B cells were expanded in medium containing IL-4 and CD40 for 24 h followed by OHT addition and further expansion for 72 h. Lysates were subjected to WB analysis (left panels). In parallel, apoptosis was detected by FACS analysis (n=3, right panels). (B) *Usp8*$^{f/f}$ and *Usp8*$^{f/f}$*Rosa26*-CreERT2 splenic B cell lysates generated as in (A) were subjected to WB with the indicated antibodies. (C) *Usp8*$^{f/f}$ and *Usp8*$^{f/f}$*Rosa26*-CreERT2 splenic B cells were expanded as in (A) and treated with the inhibitors MLN4924 (NAE inhibitor, 500 nM) and/or MLN7243 (UBA1 inhibitor, 500 nM) as indicated for 16 h before lysis and WB analysis. (D) Cell viability of KMS-18 or KMS-27 WT and BTZ-resistant mutant MM cells treated with BTZ (5 nM), DUB-IN-2 (25 µM), or a combination of both for the times indicated (n=3, 2-way ANOVA, Dunnett's post hoc test). (E, F) WB analysis of KMS-18/KMS-18-T21A (E) or KMS-27/KMS-27-A49V (F) MM cells after exposure to BTZ and/or DUB-IN-2 for the times indicated (top). Results in Fig. 4 are representative of at least 2 independent experiments.

Fig. 5. The inhibitor DUB-IN-2 exerts USP8-independent effects on cell viability. (A) Cell viability of KMS-18 or KMS-27 WT and mutant MM cells after transfection with pooled (4 individual siRNAs) non-targeting (NT) siRNA or pooled siRNA directed against USP8 for 72 hours followed by treatment with BTZ (15 nM) for the times indicated (n=3, 2-way ANOVA, Dunnett's post hoc test). (B) KMS-18-T21A mutant MM cells were transfected with siRNAs as in (A) for 96 hours followed by treatment with BTZ for 6 hours. After lysis, expression of the indicated proteins was analyzed by WB. (C) Cell viability of KMS-18-T21A mutant MM cells after transfection with pooled non-targeting (NT) siRNA, or pooled or individual siRNA_1 or siRNA_2 directed against USP8 for 72 hours followed by treatment with BTZ (25 nM) and/or DUB-IN-2 (25µM) for 24 h (n=3, 2-way ANOVA, Tukey post hoc test). (D) KMS-18-T21A mutant MM cells were transfected as in (C) and treated with BTZ (25 nM) and/or DUB-IN-2 (25µM) for 6 h. Lysates were analyzed by WB. (E) 293T cells were transfected with FLAG-WT-USP8 or FLAG-tagged USP8 with silent mutations in the siRNA2 target sequence as indicated. Transfection with USP8 siRNA2 was performed after 24h and lysates were generated after 96h and analyzed by WB as indicated. (F) WB analysis of KMS-18-T21A mutant MM cell lysates after transfection of cells with pooled NT siRNA, USP8_siRNA_2, pooled siRNA directed against CHOP, or a combination of USP8- and CHOP-specific siRNA for 72 h followed by treatment with a combination of 25 nM BTZ and 25µM DUB-IN-2 for 24 h where indicated. Arrows indicate cleaved caspases. (G) Viability of KMS-18-T21A cells transfected as in (F) followed by inhibitor treatment for 48 h. (H) KMS-18-T21A cells transfected with pooled NT siRNA or USP8 siRNA_2 for 96 h or treated with BTZ (25 nM) and/or DUB-IN-2 (25µM) for 24 h were analyzed by AO staining. Results are representative of 5 pictures taken from 2 independent experiments, respectively. (I) KMS-18-T21A cells were treated with Folimycin (100 nM) for the times indicated and lysates were analyzed by WB. (J) KMS-18-T21A mutant MM cells were treated with BTZ and/or DUB-IN-2 for 12 h. Bafilomycin (200 nM) was

added 4 h prior to lysis as indicated. Lysates were analyzed by WB. (K) Schematic representation of differentially regulated apoptosis pathways triggered by proteotoxic stress upon USP8 depletion or DUB-IN-2/BTZ treatment. WB results in Fig. 5 are representative of at least 2 independent experiments.

Fig. 6 (A) Adverse effect of low USP8 expression in MM patients at diagnosis versus effective DUB-IN-2-mediated inhibition of MM cells in mice. Kaplan Meier survival analysis of MM patients included in the MMRF CoMMpass study according to USP8 expression at time of diagnosis (Log rank test). (B) Box plot showing no significant differences of USP8 expression among patients of different MM disease stages according to Kruskal-Wallis testing. (C) Infiltration of MM cells in spleens of NSG mice that had been treated with either control (0.9NaCl/PEG300 1:1 (v/v)), BTZ (BTZ, 0.6mg/kg), or BTZ combined with DUB-IN-2 using 5mg/kg 5 times over a period of 13 days, followed by 2mg/kg twice a week in spleen. (D) Kaplan Meier plot showing the toxicity of the DUB-IN2/BTZ combination treatment (5mg/kg).

Methods

Mice. *Usp8*$^{f/f}$ [36], *Cd19*-Cre (B6.129P2(C)-*Cd19*$^{tm1(cre)Cgn}$/J) [67], *mb1*-Cre (B6.C(Cg)-*Cd79a*$^{tm1(cre)Reth}$/EhobJ) [29], *Rosa26*-CreERT2 (Gt(ROSA)26Sor$^{tm2(cre/ERT2)Brn}$) [68], and NSG (NOD.Cg-*Prkdc*^{scid} *Il2rg*^{tm1Wjl}/SzJ, JAX stock #005557) [69] mice have been described. Mice used for experiments were 8-12 weeks old and on the C57BL/6 background. For histology, B cell enrichment, or if paired T-tests were performed, sex-matched littermates were used. Animals were housed in a specific pathogen-free barrier facility according to the protocols of the Center for Experimental Models and Transgenic Service at the University Clinic in Freiburg or at the RWTH University Aachen. All experiments were approved by national authorities and the ethics review board for animal studies at the University of Freiburg or RWTH University Aachen.

Southern blot analysis. LoxP-flanked and deleted *Usp8* alleles were identified by Southern blot analysis of NcoI fragments of genomic DNA as described [36].

Cell preparation and flow cytometry. Spleens, lymph nodes, and thymi were mashed into single-cell suspensions in FACS buffer (PBS containing 1-2% FCS). Bone marrow was obtained from tibias and femurs by flushing with FACS buffer. Peritoneal cavity cells were harvested post-euthanasia by i.p. injection of FACS buffer and peritoneal massage. Splenocytes and BM cells were depleted of red blood cells with RBC lysis buffer (Sigma or BioLegend). Cell suspensions were incubated with mouse Fc Block (BD or BioLegend). B cells were isolated from Spleen using biotinylated anti-CD19 antibody (BD Pharmingen, clone ID3) or the BD IMag^{TM} Biotinylated Mouse B Lymphocyte Enrichment Cocktail and BD IMAG^{TM} Streptavidin Particles Plus. T cells were isolated using the BD IMag^{TM} Biotinylated Mouse CD4 T lymphocyte enrichment Cocktail

and BD IMAG™ Streptavidin Particles Plus. DAPI or Zombie UV fixable viability dye (Biolegend) were used for live/dead discrimination. Expression of surface and intracellular markers was analyzed with a flow cytometer (Becton Dickinson FACS Calibur, BD FACSCanto II, or BD Fortessa SORP) and FlowJo software. Annexin V/PI staining was performed using the eBioscience Annexin V apoptosis detection kit APC.

Cell culture, proliferation, activation, and viability. For the proliferation experiments, purified B cells ($5x10^4$ per well) were stimulated by incubation with 5 µg ml^{-1} anti-IgM $F(ab')_2$ fragment antibody (115-006-020; Jackson Immuno Research) with or without 5 µg ml^{-1} anti-CD40 antibody (553787, BD Pharmingen), with 100 ng/ml MPL-A (Invivogen) or 100 nM CpG (ODN 1668, Invivogen). B cell proliferation was quantified after 36 h using the Cell Proliferation ELISA, BrdU (colorimetric) from Roche. For short-term stimulation, B cells were starved for 2 h in RPMI1640 medium containing 0.2% bovine serum albumin without FCS and activated by preincubation with 10 µg ml-1 anti-IgM for 30 min on ice and stimulation for the times indicated at 37°C. T cells were starved for 2 h in RPMI1640 medium without FCS. T cells were activated by pre-incubation on ice for 30 min with soluble anti-mouse CD3ε antibody (10µg ml^{-1}; 145-2C11; eBioscience) and anti-mouse CD28 antibody (2µg ml^{-1}; 37.51, eBioscience), followed by stimulation for the appropriate time at 37°C with pre-warmed anti-hamster IgG1 antibody (5µg ml^{-1}; G94-56, BD Pharmingen). *Ex vivo* expansion of B cells was performed using recombinant murine IL-4 (100 u ml^{-1}, Peprotech) and anti-mouse CD40 antibody (5 µg ml^{-1}; HM40-3, Biolegend), or anti-IgM $F(ab')_2$ fragment (5 µg ml^{-1}) and anti-CD40 antibody (2.5 µg ml^{-1}). OHT (1 µM, Sigma) was added 24 h post B cell isolation and stimulation. DUB-IN-2 (25 µM, MedChem Express) and BTZ (5 t0 25 nM, Selleckchem) were added for the times indicated before analysis. Cell viability was analyzed using

the XTT cell proliferation kit II (Roche Diagnostics). Drug treatment was started 24 h after cell seeding. Absorbance was measured as indicated and normalized to the respective controls.

Single cell RNA-seq analysis. Single cell RNA-seq analysis was performed with splenic B cells enriched from *Usp8*$^{f/f}$ and *Usp8*$^{f/f}$*Cd19*-Cre mice using the BD IMag™ Biotinylated Mouse B Lymphocyte Enrichment Cocktail and BD IMAG™ Streptavidin Particles Plus (n=3). For single cell library preparation, cells were loaded onto a Chromium Single Cell 3′ G Chip (10X Genomics) according to the manufacturer's instructions without modifications using Chromium Next GEM Single Cell 3' Reagents Kit v3.1 (10x Genomics). The 6 samples were multiplexed using Cell Multiplex Oligos (CMOs) for CellPlex reagents. Dual Index Plate NN Set A (10x Genomics) was used for Cell Multiplexing library construction, Dual Index Plate TT Set A was used for Gene Expression library construction according to the manufacturer's instructions. The cDNA content and size of post-sample index PCR samples was analyzed using a 2100 BioAnalyzer (Agilent). Library quantification was done using NEB Next® Library Quant Kit for Illumina® (New England Biolabs) following manufacturer's instructions. Sequencing libraries were loaded onto an Illumina NextSeq 1000 P2 flow cell, with sequencing settings according to the recommendations of 10x Genomics (read 1: 28 cycles, read 2: 90 cycles, i7 index: 10 cycles, i5 index: 10 cycles). Cell Ranger v6.1.2 software was used to align the sequencing data to the mouse genome mm10. The indexed mouse genome used for alignment was downloaded from 10x genomics (refdata-gex-mm10-2020-A).

The single cell data were loaded into R and in a Seurat object (v.4) for subsequent bioinformatics analysis. Cells with a high mitochondrial content (> 20%) or low number of genes detected (<200) were discarded. SoupX [70] was used to estimate and remove cells contaminated from ambient mRNA and ALRA [71] was used for data imputation.

The data were normalized with the "LogNormalized" method and scaled. The top 10.000 variable genes were used for the Principal Component Analysis and the UMAP was generated using the top 20 principal components. The Louvain algorithm with resolution=0.8 from the FindClusters function was used to assign clusters to cells in an unbiased way. Cell type annotation was performed using the markers reported by Nguyen et al. [30] and clusters were merged when no relevant difference in marker expression was detected. Other bioinformatics analyses and data visualization were performed with the other Seurat or ggplot2 functions. The data are available at https://www.ncbi.nlm.nih.gov/geo/query/acc.cgi?acc=GSE244334 (access token available upon request). Pathway enrichment analysis was performed with ReactomePA v1.46.0 (10.1039/c5mb00663e). Genes with adjusted p value < 0.1 and log2FC > 0 or <0 were selected to perform the enrichment analysis for pathways upregulated in the *Usp8*$^{f/f}$*Cd19* B cell/PC and control samples, respectively. Pathways that had 70% of overlapping genes were removed from the final results in order to remove redundancy.

Cell lines, expression constructs, transfection and inhibitor treatment. NP-specific mIgM-BCR–expressing transfectant K46Lμm of the mouse B cell line K46 [72,73] were obtained from W. Schamel, Freiburg. The human MM cell lines KMS-18 and KMS-27 and the mutant T21A and A49V derivatives expressing PSMB5 with a substitution in the BTZ binding cleft were described previously [51]. Human and mouse USP8 tagged with FLAG at the carboxyl terminus were expressed via the vector pFLAG-CMV5a and the retroviral expression vector MIEG3, respectively. Retroviral particles were produced in Platinum-E retro-viral packaging cells according to standard protocols. Mammalian expression vectors for HA-NEDD8 and HA-SENP8 were purchased from addgene. Point mutations were generated by site-directed mutagenesis with the QuikChange mutagenesis system (Stratagene). HEK293T cells were transfected with FuGENE HD Transfection

Reagent from Roche and were harvested 36 h post transfection. The NEDD8-activating enzyme (NAE) inhibitor MLN4924 (LKT Laboratories), the UBA1 inhibitor MLN7243 (MedChemExpress), Folimycin (MedChemExpress), BTZ (Selleckchem), and DUB-IN-2 (MedChemExpress) were applied to cells as indicated in the figure legends. ON-TARGETplus SMARTpool siRNA directed against human USP8 and CHOP, individual siRNAs directed against USP8 (Target Sequence siRNA_1: GGCAAGCCAUUUAAGAUUA; siRNA_2: CCACUAGCAUCCACAAGUA), and ON-TARGETplus Non-targeting (NT) Pool siRNA were purchased from Dharmacon. SiRNA transfections were perfomed using Lipofectamine® RNAiMAX reagent according to manufacturer's instructions. For rescue of USP8 depletion by siRNA_2, the respective target sequence was mutated as follows: CCCCUAGCUUCCACAAGUA.

Immunoblot analysis and immunoprecipitation. Cells were lysed in DDM lysis buffer (50 mM Tris-HCl, pH 7.4; 150 mM NaCl; 1 mM EDTA; 50 mM NaF; 1mM sodium vanadate; 1x Roche Complete Protease Inhibitor Cocktail; and 0.2% n-dodecyl-β-D-maltoside). Immunoprecipitation was performed with anti-FLAG M2 Affinity Gel (Sigma) or rat monoclonal antibody to hemagglutinin (HA) affinity matrix (3F10; Roche). Immunoblot analysis was performed with antibodies listed in Supplementary Table S1.

Conjugation and deconjugation assays. For the PRG probe conjugation assay, protein lysate was diluted 1:8 in 25 µl assay buffer (50 mM Na_2HPO_4; 500 mM NaCl; 10mM DTT; pH7.9) containing 2 µg NEDD8-PRG or 5µM Bt-Ub-PRG and incubated for 2 h at 37°C. To test the deconjugation capacity of USP8 towards mixed ubiquitin/NEDD8 chains, 5µl protein lysate generated with DDM

lysis buffer w/o proteinase inhibitors was incubated with 365 ng recombinant USP8 in PBS containing 5mM $MgCl_2$ and 2mM DTT for 1 h at 37°C.

ELISA, T cell dependent and independent Ig responses, cytokine bead array. Basal immunoglobulin levels in mouse plasma were analyzed by Aushon Biosystems, Billerica, MA. *Usp8*$^{f/f}$ and *Usp8*$^{f/f}$*Cd19*-Cre mice have been i.p. injected with 50 µg TNP-KLH (Biosearch Technologies) precipitated in alum (TD response) or with 25 µg TNP-Ficoll (Biosearch Technologies, TI response) and blood was collected at day 0 and days 7, 14, and 28 post injection. TNP-specific IgM, IgG1 and IgG3 levels in the plasma were quantified using the SBA Clonotyping™ System/AP from SouthernBiotech. Detection of serum cytokine levels was performed using mouse enhanced sensitivity Master buffer Kit (562246, Becton Dickinson) along with Flex Kits for TNF (562336), IL-6 (562236) and IL-1beta (562278) according to manufacturer's recommendations.

Ca^{2+} flux. B cells were purified, starved of serum as described above and loaded for 30 min at 37°C with Indo-1-AM (5µg/ml) in RPMI-1640 medium without FCS. Stimulation with anti-IgM (5µg/ml; identified above) was carried out in RPMI-1640 medium with 10% FCS. The emission wavelength ratios of intracellular Ca^{2+}-bound and unbound Indo-1-AM were analyzed on a LSRII flow cytometer with FACSDiva software (BD Biosciences).

Immunohistochemistry and acridine orange (AO) staining. Hematoxilin and eosin staining and immune histological staining of splenic paraffin or cryosections with antibodies was carried out with the appropriate antibodies (dilution 1:500, except for CD3: 1:100; anti-B220: 1:200; Ki67: 1:50; PNA: 1:250) (Supplementary Table S1) as described previously [22,74]. In brief, spleens were

removed and fixed in 4 % buffered formalin. Paraffin-embedded 3 µm sections were deparaffinized and were incubated in 3 % H_2O_2 in methanol and subsequently in 70 % ethanol. Cryosections were fixed for 5 min in ice-cold acetone, followed by incubation with 10% FCS in PBS. Spleen sections were incubated with the primary antibodies overnight. Secondary antibodies and fluorescence labelled streptavidin (1:500) were added for 2 h at room temperature. Images were taken using a conventional fluorescence microscope (Olympus BX-61). Cells were stained in AO (100 ng/ml, Invitrogen) according to manufacturer's instructions. Live cell imaging was performed at 37°C in a 5% CO2 humidified atmosphere with a Leica SP8 confocal microscope equipped with a 63×/1.40 and 40×/1.25 oil objective (Leica Microsystems). Laser settings were kept constant for each experiment to allow direct comparison of signal intensities between images of the same channel.

Generation of stable GFP expressing cell lines

KMS-18 and KMS-18-T21A cell lines were seeded at $1x10^5$ in 200µl medium (RPMI 1640 supplemented with 10% Fetal Bovine Serum, without antibiotics) and mixed with polybrene (16µg/ml, Sigma-Aldrich). Cells were then placed in a 48-well plate (Thermo Fisher Scientific) together with the virus particles (Firefly luciferase-GFP lentivirus, System Biosciences, stock: 21,9 TU/ml, MOI 10). The plate was centrifuged for 2h at 1200g and 32°C. After centrifugation, cells were expanded for 5 days (37 °C and 5% CO2) in the presence of puromycin (2 µg/ml) and the GFP positive cells were isolated by flow cytometry.

Transplantation of NSG mice

$1x10^6$ multiple myeloma KMS-18 or KMS-18-T21A cells, combined with $5x10^5$ HS27a human stromal cells were transplanted into 9 -week-old NOD/Scid/IL2Rγ-/- (NSG) mice (Charles River) after sublethal irradiation with 240 cGy (2,4Gy) using MultiRad 225 (Cu 0,3mm filter). To prevent

infections, cotrimoxazol (100 µg/ml) was added to the drinking water for 2 weeks after transplantation. Bortezomib was administered twice per week (i.p.) at a concentration of 0,6mg/kg and DUB-IN-2 solved in 0.9% NaCL/PEG300 1:1 (v/v) was administered 2-5 times per week (i.p.) at concentrations of 2-5 mg/kg. As control we administered 0.9% NaCL/PEG300 1:1 (v/v).

Chemical synthesis of K48-ubiquitinated-NEDD8 and K48-diubiquitin. K48-ubiquitinated-NEDD8 and K48-diubiquitin were chemically synthesised as described by El Oualid et al. [75]. In brief, Ubiquitin$_{1-76}$-thioester and K48-γ-thiolysine- Ub or NEDD8 were prepared using automated solid phase peptide synthesis. The StBu protected K48γ-thiolysine-Ub or NEDD8 (5 mg) was dissolved in 50 µL DMSO and added to 600 µL 8 M Gdn.HCl/100 mM phosphate buffer at pH 7.6 supplemented with 50 µL 1 M TCEP and reacted at 37 ^{0}C. After LC-MS analysis revealed complete deprotection of the thiolysine, 1.25 equivalent of Ub-thioester dissolved in 50 µL DMSO and 50 uL 1M MPAA were added. The pH was re-adjusted to 7.6 and the reaction was performed for 2 hours at 37 ^{0}C. Following RP-HPLC purification the appropriate fractions were lyophilized. The lyophylised diUb(l) (1.5 mg) was desulfurized by dissolving in 25 µL DMSO and subsequent dilution into 600 µL 8 M Gdn.HCl/100 mM phosphate buffer at pH 7.6 and 150 µL 1M TCEP. VA044 (25 mg/mL) and GSH (25 mg/mL) were added, the pH was adjusted to 7.0 and the reaction was agitated for 16 hours at 37 ^{0}C. Following RP-HPLC purification the appropriate fractions were lyophilized. The lyophilized diUb(l) was dissolved in 25 µL DMSO and diluted into 750 µL 20 mM TRIS, 150 mM NaCl at pH 7.6 and purified on a S75 10/300 sephadex size exclusion column (GE Healthcare). Appropriate fractions were collected and pooled. Spin-filtration (Amicon 3 kD MWCO) was used to concentrate the sample to 3.4 mg/mL, based on nanodrop analysis (M.W.: 17089 Da, ε_{280}: 4470 $M^{-1}cm^{-1}$). The aliquots were snap frozen and stored at -80 ^{0}C until further use.

HRMS-measurements. High resolution mass spectra were recorded on a Waters Acquity H-class UPLC with XEVO-G2 XS Q-TOF mass spectrometer equipped with an electrospray ion source in positive mode (source voltage 3.0 kV, desolvation gas flow 900 L/hr, temperature 250°C) with resolution R = 22000 (mass range m/z = 50-2000) and 200 pg/uL Leu-Enk (m/z = 556.2771) as a lock mass. Data processing was performed using Waters MassLynx MS Software 4.1 (deconvolution with MaxEnt1 function).

K48-ubiquitinated-NEDD8: HR-MS analysis for $C_{757}H_{1266}N_{208}O_{234}S_2$: Deconvoluted ESI MS^+ (amu) calcd: 17089.5, found 17089.0, rt: 1.35 min.

K48-diubiquitin: HR-MS analysis for $C_{757}H_{1258}N_{210}O_{235}S$: Deconvoluted ESI MS^+ (amu) calcd: 17093.7, found 17095.0, rt: 1.36 min.

DUB cleavage assays. USP8 (human, full length, Ubiquigent 64-0053-050) was diluted to a final concentration of 40 nM in buffer containing 20 mM Tris·HCl, 150 mM NaCl, pH 7.6 and 5 mM DTT. Subsequently 5 µM synthetic K48-ubiquitinated-NEDD8 or K48-diubiquitin were added. The samples were incubated at 37°C for 30, 60 and 120 minutes. At the indicated time the reaction mixture was diluted with sample buffer (3x) (containing 75% NUPAGE® LDS sample buffer (4x, Invitrogen), 7.5% β-mercaptoethanol and 17.5% water), and loaded on 12% NUPAGE® Novex® Bis-Tris Mini Gels (Invitrogen) using MES-SDS as running buffer. SeeBlue Pre-stained Standard (Invitrogen, LC5925) was used as molecular weight marker. Gels were stained using InstantBlue™ (Expedeon) and scanned using a GE Healthcare Amersham Imager 600.

Ubiquitination proteomics.

Sample preparation for pull down-MS experiments.

In the pull down-MS experiments, after immunoprecipitation beads were washed 2 times with DDM lysis buffer and three times with trypsin buffer containing 20 mM Tris HCl, pH 8.0; 2 mM $CaCl_2$. The proteins were on-bead digested with 1 µg trypsin (Promega) for 4 hours at 37 ˚C under agitation. Then, the beads were precipitated and the supernatants were mixed with another 1 µg of trypsin and further digested overnight at 37°C under agitation. Peptides were desalted on reversed phase C18 OMIX tips (Agilent), dried under vacuum in HPLC inserts and stored at −20 °C until LC-MS/MS analysis.

Sample preparation for GlyGly(K) sites identification by MS.

200 x 10^6 K46Lµm cells were homogenized in 10 mL urea lysis buffer containing 9 M urea; 20 mM HEPES, pH 8.0. Samples were sonicated by three pulses of 10 s at an amplitude of 20% and centrifuged for 15 min at 16,000 × g at room temperature to remove insoluble components. The protein concentration in the supernatants of each replicate was measured using a Bradford assay (Biorad) and equal protein amounts, each containing 10 mg total protein, were used for further analysis. Proteins in each sample were reduced by adding 5 mM DTT and incubation for 30 min at 55 °C. Alkylation of the proteins was done by addition of 10 mM chloroacetamide and incubation for 15 min at room temperature in the dark. Next, samples were diluted with 20 mM HEPES, pH 8.0 to an urea concentration of 4 M and proteins were digested with 40 µg endopeptidase LysC (Promega) (1/250, w/w) for 4 h at 37 °C. Samples were further diluted with 20 mM HEPES pH 8.0 to a urea concentration of 2 M and proteins were digested with 50 µg trypsin (Promega) (1/200, w/w) overnight at 37 °C. Immunocapture of GG-modified peptides was then performed using the PTMScan® Ubiquitin Remnant Motif (K-ε-GG) Kit (Cell Signaling Technology) according to the manufacturer's instructions. Briefly, peptides were purified on Sep-Pak C18 cartridges (Waters),

lyophilized for 2 days and re-dissolved in 1.4 ml 1x immunoprecipitation buffer supplied with the kit. Note that at this point, aliquots corresponding to 50 µg of digested protein material were taken for shotgun proteomics analysis. Peptides were incubated with the antibody-bead slurry for 2 h on a rotator at 4 °C and after several wash steps, GG-modified peptides were eluted in 100 µl 0.15% TFA and desalted on reversed phase C18 OMIX tips (Agilent). Purified GlyGly-K modified peptides were dried under vacuum in HPLC inserts and stored at −20 °C until LC-MS/MS analysis.

LC-MS/MS.

GlyGly-K modified peptides isolated from B cells shown in Figure 3A were re-dissolved in 20 µL loading solvent A (0.1% TFA in water/ACN (98:2, v/v)) of which 10 µL were injected for LC-MS/MS analysis on an Ultimate 3000 RSLCnano system (ThermoFisher scientific) in-line connected to a Q Exactive HF mass spectrometer (Thermo). Trapping was performed at 10 µL/min for 4 min in loading solvent A on a 20 mm trapping column (100 µm internal diameter (I.D.), 5 µm beads, C18 Reprosil-HD, Dr. Maisch, Germany). Peptides were separated on a 200 cm long micro pillar array column (µPAC™, PharmaFluidics) with C18-endcapped functionality. This column consists of 300 µm wide channels that are filled with 5 µm porous-shell pillars at an inter pillar distance of 2.5 µm. With a depth of 20 µm, this column has a cross section equivalent to an 85 µm inner diameter capillary column. Peptides isolated from B cells were eluted from the analytical column by a non-linear gradient from 2 to 55% solvent B (0.1% FA in water/acetonitrile (2:8, v/v)) over 120 minutes at a constant flow rate of 300 nL/min, followed by 20 min in 99% solvent B. The column was then re-equilibrated with 98% solvent A for 10 min. For the analyses of peptides isolated from B cells, the column temperature was kept constant at 50 °C in a column oven (CoControl 3.3.05, Sonation). The mass spectrometer was operated in positive and data-dependent mode, automatically switching between MS and MS/MS acquisition for the 8 most abundant ion peaks per MS spectrum for the analyses of the peptides isolated from B cells. Full-scan MS spectra

(375–1,500 m/z) were acquired at a resolution of 60,000 (at 200 m/z) in the orbitrap analyzer after accumulation to a target value of 3E6 for a maximum of 60 ms. The most intense ions above a threshold value of 8.3E3 were isolated in the trap with an isolation window of 1.5 Da for maximum 120 ms to a target AGC value of 1E5 for the analysis of peptides isolated from B cells. Only precursor ions with a charge state from 2 to 6 were selected for MS/MS. Peptide match was set on "preferred" and isotopes were excluded. Dynamic exclusion time was set to 12 s. Fragmentation was performed at a normalized collision energy of 28%. MS/MS spectra (200-2,000 m/z) were acquired at fixed first mass 145 m/z at a resolution of 15,000 (at 200 m/z) in the Orbitrap analyzer. MS/MS spectrum data type was set to centroid. The polydimethylcyclosiloxane background ion at 445.12003 was used for internal calibration (lock mass).

Dried peptides of the shotgun aliquots were re-dissolved in loading solvent A (0.1% TFA in water/ACN (98:2, v/v)) and 3 µg peptides of each sample was injected for LC-MS/MS analysis on an Ultimate 3000 RSLC nanoLC (Thermo Scientific, Bremen, Germany) in-line connected to an LTQ-Orbitrap Elite (Thermo Fisher Scientific, Bremen, Germany) equipped with a pneu-Nimbus dual ion source (Phoenix S&T). Trapping was performed at 10 µL/min for 4 min in solvent A on a 20 mm trapping column (made in-house, 100 µm internal diameter (I.D.), 5 µm beads, C18 Reprosil-HD, Dr. Maisch, Germany) and the sample was loaded on a reverse-phase column (made in-house, 75 µm I.D. x 250 mm length, 1.9 µm beads C18 Reprosil-HD, Dr. Maisch). Peptides were eluted by a non-linear increase from 1 to 56% MS solvent B (0.1% FA in water/ACN (2:8, v/v)) over 145 minutes, at a flow rate of 250 nL/min, followed by a 15-minutes wash reaching 99% MS solvent B and re-equilibration with MS solvent A (0.1% FA in water/ACN (2:8, v/v)). The mass spectrometer was operated in data dependent, positive ionization mode, automatically switching between MS and MS/MS acquisition for the 20 most abundant peaks in a given MS spectrum. The source voltage was 3.1 kV, and the capillary temperature was 275°C. In the LTQ-

Orbitrap Elite, full scan MS spectra were acquired in the Orbitrap (m/z 300−2,000, AGC target 3 × 10^6 ions, maximum ion injection time 100 ms) with a resolution of 60 000 (at 400 m/z). The 20 most intense ions fulfilling predefined selection criteria (AGC target 5 × 10^3 ions, maximum ion injection time 20 ms, spectrum data type: centroid, exclusion of unassigned and 1 positively charged precursors, dynamic exclusion time 20 s) were then isolated in the linear ion trap and fragmented in the high pressure cell of the ion trap. The CID collision energy was set to 35% and the polydimethylcyclosiloxane background ion at 445.120028 Da was used for internal calibration (lock mass).

For the pulldown-MS analyses shown in Figure 3E, dried peptides were re-dissolved in 20 µl loading solvent A of which 13 µL were injected for LC-MS/MS analysis as described for the analysis of peptides isolated from B cells. Peptides were eluted from the analytical column by a non-linear gradient from 2 to 56% solvent B over 150 minutes at a constant flow rate of 250 nL/min, followed by 10 min in 99% solvent B and the column was then re-equilibrated with 98% solvent A for 25 min. The column was then re-equilibrated with 98% solvent A (0.1% FA in water) for 20 min. The column temperature was kept constant at 50 °C in a column oven (CoControl 3.3.05, Sonation). The mass spectrometer was operated in positive and data-dependent mode, automatically switching between MS and MS/MS acquisition for the 16 most abundant ion peaks per MS spectrum. Full-scan MS spectra (375–1,500 m/z) were acquired at a resolution of 60,000 (at 200 m/z) in the orbitrap analyzer after accumulation to a target value of 3E6 for a maximum of 60 ms. The most intense ions above a threshold value of 1.3E4 were isolated in the trap with an isolation window of 1.5 Da for maximum 80 ms to a target AGC value of 1E5.

For the pull down-MS analyses shown in Figure 3H, dried peptides were re-dissolved in 20 µl loading solvent A of which 5 µL were injected for LC-MS/MS analysis as described above for the analysis of peptides isolated from B cells. Peptides were eluted from the analytical column as

described for the analysis of peptides isolated from B cells, but over a gradient for 90 minutes. The column temperature was kept constant at 50 °C in a column oven (CoControl 3.3.05, Sonation). The mass spectrometer was operated as described above, but only the top 12 most abundant ion peaks were fragmented per MS spectrum. Fragmentation was performed as described for the analysis of peptides isolated from B cells but the dynamic exclusion time was set to 20 s.

LC-MS/MS data analysis.

Data analysis was performed with MaxQuant (version 1.5.7.4, 1.5.8.3, 1.6.1.0 or 1.6.11.0) using the Andromeda search engine with default search settings including a false discovery rate set at 1% on both the peptide and protein level. The analysis of the B cells shown in Figure 3B was performed with two different searches to analyze the spectra generated from the analysis of the GlyGly-K enriched samples and the shotgun samples. Spectra from the pull down-MS shown in Figure 3E were searched twice: for the identification of GlyGly-K modified peptides and for the identification of proteins. Spectra from the pull down-MS shown in Figure 3H were searched once: for the identification of GlyGly-K modified peptides. Spectra were interrogated against proteins in the Uniprot/Swiss-Prot database ([www.uniprot.org]). The database released on January 2018 containing 16,946 mouse protein sequences were used for the analysis of Fig. 3B. The database released on September 2017 or January 2020 containing 20,226 or 20,595 human protein sequences was used for the pulldown-MS shown in Figure 3E and 3H, respectively. Mass tolerance for precursor ions was set to 4.5 ppm for all analysis. Mass tolerance for fragment ions was set to 20 ppm (orbitrap analyzer) for the analysis of the GlyGly-K modified peptides and the pulldown-MS, while it was set to 0.5 Da (ion trap analyzer) for the shotgun samples. Enzyme specificity was set as C-terminal to arginine and lysine (trypsin), also allowing cleavage at arginine/lysine–proline bonds with a maximum of three missed cleavages for the identification of GlyGly-K modified peptides or set to two missed cleavages for the identification of protein. Carbamidomethylation of

cysteine residues was set as a fixed modification in the analyses of B cells. In all analyses, variable modifications were set to oxidation of methionine (to sulfoxides) and acetylation of protein N-termini. To identify GlyGly-K modified peptides, GlyGly modification of lysine residues was set as an additional variable modification. In the pulldown-MS, phosphorylation of Serine, Threonine or Tyrosine was set as an additional variable modification. Score for modified peptides was set to 40 or 30 for the identification of proteins or GlyGly-K modification sites, respectively. In the pulldown-MS shown in Figure 3E, score for modified peptides was set to 35 for the identification of proteins and GlyGly-K modification sites. In all searches, matching between runs was enabled with an alignment time window of 20 min and a matching time window of 1 min. Only proteins with at least one peptide were retained to compile a list of identified proteins. In the analysis of B cells, 3,273 mouse proteins, and 7,933 GG-modification sites were identified. In the pulldown-MS shown in Figure 3E, 1,389 human proteins and 126 GG-modification sites were identified. In the pulldown-MS shown in Figure 3H, 4,417 human proteins and 554 GlyGly-K modification sites were identified. Proteins were quantified by the MaxLFQ algorithm integrated in the MaxQuant software. A minimum of two ratio counts from at least one unique peptide was required for quantification in all analyses except for the pulldown-MS for which a minimum of two ratio counts from at least one unique or razor peptide was required.

Further data analysis was performed with the Perseus software (version 1.5.5.3, 1.6.1.1 or 1.6.2.3). For the analysis of the shotgun data, the proteinGroups table from MaxQuant was loaded in Perseus, reverse database hits were removed as well as proteins only identified by sites. The LFQ intensities were log2 transformed and replicate samples were grouped as above. Proteins with less than three valid values in at least one group were removed and missing values were imputed from a normal distribution around the detection limit. To reveal the proteins that were significantly regulated, sample groups were defined based on genotype (WT-USP8 vs. $USP8_{C748A}$) and a t-test

(FDR = 0.05 and S0 = 1) was performed to compare the intensity of the proteins between the two genotypes. Quantified proteins (n = 2,251) and the results of the t-tests are shown in Figure 3B. For the analysis of GlyGly-K modification sites, the GlyGly (K) Sites table from MaxQuant was loaded and reverse database hits were removed. The site table was expanded, intensities were log2 transformed and normalized for each sample by subtracting the median intensity. Replicate samples were grouped, sites with less than three valid values in at least one group were removed, and missing values were imputed from a normal distribution around the detection limit. To reveal sites that were significantly regulated, sample groups were defined based on genotype (WT-USP8 vs. $USP8_{C748A}$) and a t-test (FDR = 0.05 and S0 = 1) was performed to compare the intensities of the sites between the two genotypes. Quantified GlyGly-K modified sites (n = 5,824) and the results of the t-tests are shown in Figure 3B. In all analyses, the same workflow as described above was applied for the analysis of GlyGly-K modification sites or for the analysis of proteins. For the pulldown-MS analysis shown in figure 3E, 845 proteins 49 GG-modification sites were evaluated. For the pulldown-MS analysis shown in Figure 3H, only identified GlyGly-K modification sites that are derived from NEDD8 or Ubiquitin proteins were displayed in the heatmap.

All MS proteomics data have been deposited to the ProteomeXchange Consortium via the PRIDE partner repository. The Shotgun analysis and the anlysis of GlyGly-K modification sites shown in Figure 3B were registered under the data set identifier PXD024395 (Username: reviewer_pxd024395@ebi.ac.uk; Password available upon request). The pull down-MS analysis shown in Figure 3E was registered under the data set identifier PXD024755 (Username: reviewer_pxd024755@ebi.ac.uk; Password available upon request). The pull down-MS analysis shown in Figure 3H was registered under the data set identifier PXD024429 (Username: reviewer_pxd024429@ebi.ac.uk; Password available upon request).

Statistical analysis. We ensured that our sample sizes matched those generally used in the field. T-testing, or 2-way ANOVA and Dunnett's or Tukey post hoc tests were applied and differences with a P value of <0.05 were considered significant. Excel and GraphPad Prism 10 were used for statistical testing if not mentioned otherwise.

The transcriptomic data and clinical data of the Multiple Myeloma Research Foundation (MMRF) CoMMpass study was retrieved from the Genomic Data Commons (GDC) data portal. Raw Counts were normalized using the Trimmed Mean of M-values (TMM) normalization (Robinson 2010, Genome biology). The remaining samples were sorted according to the expression of USP8 and were stratified in three groups: Low expression (bottom 35%), Mid expression (between 35% and 65%), Top expression (above 65%). Kaplan-Meier overall survival plots on these three groups of samples were generated using the function TCGAanalyze_survival from the R package TCGAbiolinks v2.30 [76].

The boxplot with patients stratified by International Staging System (ISS) was generated using ggplot2 v3.4.4 and ggpubr v0.6.

Supplemental Information

Fig. S1. (A) Marginal GADS expression in B cells as compared to T cells. Splenic T and B cells were enriched and stimulated for the times indicated with anti-CD3/CD28 or anti-IgM antibodies, respectively. USP8, GADS, 14-3-3β, phospho-ERK1/2 and Actin expression were determined by WB. (B) Verification of *Usp8* gene deletion in B cells of *Usp8*$^{f/f}$*Cd19*-Cre mice. Southern blot analysis of NcoI-digested genomic DNA from *Usp8*$^{f/f}$ control and *Usp8*$^{f/f}$*Cd19*-Cre B cells reveals efficient *Usp8* gene recombination. Deletion is indicated by a 6kb band representing the deleted allele. The 5kb band represents the floxed allele. (C) USP8 and actin expression in splenic B cells were analyzed by WB. (D) Defect in B cell development in *Usp8*$^{f/f}$*Cd19*-Cre mice as compared to *Usp8*$^{+/+}$*Cd19*-Cre control mice. Flow cytometry analysis of B cell subsets in spleen, LN, and BM of *Usp8*$^{+/+}$*Cd19*-Cre mice and *Usp8*$^{f/f}$*Cd19*-Cre mice. Pre-gating is indicated at the upper left of the FACS plots. Results are representative of 4 independent experiments. (E) Elevated percentages of B1 cells among *Usp8*$^{f/f}$*Cd19*-Cre IgM^{+} B cells. Flow cytometry analysis of B1a and B1b cell subsets in spleen and peritoneal cavity (PCav), and B2 cell subsets in PCav of *Usp8*$^{+/+}$*Cd19*-Cre and *Usp8*$^{f/f}$*Cd19*-Cre mice. Pre-gating is indicated at the upper left of the FACS plots. The percentages and total numbers of B1 and B2 cell subsets are shown on the right (unpaired, 2-sided t-test; n=4). (F-H) Altered spleen architecture and inhibition of B cell proliferation in *Usp8*$^{f/f}$*Cd19*-Cre mice. (F) Immunohistochemistry staining of paraffin-embedded spleen sections with hematoxylin/eosin (H&E), anti-B220, and anti-CD3 (brown) (scale bar 200 µm), and co-staining of frozen spleen sections as indicated (scale bar 100 µm). (G) Proliferation (BRDU incorporation) of purified splenic CD19^{+} *Usp8*$^{f/f}$ and *Usp8*$^{f/f}$*Cd19*-Cre B cells stimulated with anti-IgM in the absence or presence of anti-CD40, or with the TLR4 and TLR9 agonists "synthetic Monophosphoryl Lipid A" (MPLA) and CpG, respectively (paired, 2-sided t-test). (H) Quantification of Ki67^{+} *Usp8*$^{f/f}$ and *Usp8*$^{f/f}$*Cd19*-Cre B cells in proliferating Ki67^{+} B cell areas

(unpaired, 2-sided t-test, n≥10). Scale bar, 100µm. (I) Defect in B cell development of *Usp8*$^{f/f}$mb1-Cre mice as compared to *Usp8*$^{+/f}$mb1-Cre control mice. B cell subsets in BM, spleen, LN, and PCav of *Usp8*$^{+/f}$mb1-Cre mice and *Usp8*$^{f/f}$*mb1*-Cre mice were analyzed by flow cytometry. Pre-gating is indicated at the upper left of the respective FACS plots. Results are representative of 3 independent experiments.

Fig. S2.

Altered B cell subsets, but normal myeloid and T cell distribution, and inflammatory blood cytokine levels in B cell-specific Usp8 KO mice. (A) UMAP projection of B cell enriched splenocytes colored by graph-based clusters. (B) Flow cytometry analysis of splenic myeloid cells derived from *Usp8*$^{f/f}$ and *Usp8*$^{f/f}$*Cd19*-Cre mice. (C) Expression scores based on Mann-Whitney U statistic of 10 genes specific for the cell type reported [30] in UMAP projection. (D) Volcano plots of differential gene expression analysis of MZB, FoB, PC, and GC-like B cells. Red dots indicate significance for adjusted P value and $\log_2$ fold change. (E) Flow cytometry analysis of splenic T cell subsets derived from *Usp8*$^{f/f}$ and *Usp8*$^{f/f}$*Cd19*-Cre mice. nT, naïve T cells; TEM, effector memory T cells; Treg, regulatory T cells. (F) Inflammatory cytokine levels in serum of *Usp8*$^{f/f}$ and *Usp8*$^{f/f}$*Cd19*-Cre mice.

Fig. S3. *Cd19*-Cre-mediated deletion of USP8 alters splenic B cell compartment signaling. (A) *Usp8*$^{f/f}$ and *Usp8*$^{f/f}$*Rosa26*-CreERT2 splenic B cells were expanded in medium containing IL-4 and CD40 for 24 h followed by OHT addition and further expansion for 48 h or 72 h. Lysates were subjected to WB analysis. Results are representative of at least two independent experiments. (B) Elevated JNK activation in *Usp8*$^{f/f}$*Cd19*-Cre B cells. Splenic *Usp8*$^{f/f}$ and *Usp8*$^{f/f}$*Cd19*-Cre B cells were purified with biotinylated anti-CD19 antibodies and IMag Streptavidin Particles plus-DM,

starved for 2 hours, stimulated for the indicated times with anti-IgM $F(ab')_2$ fragment antibody, and analyzed by WB. Results are representative of 3 independent experiments. (C) Ca^{2+} influx in anti-IgM-stimulated B cells. Splenic *Usp8*$^{f/f}$ and *Usp8*$^{f/f}$*Cd19*-Cre B cells were purified as in (B), loaded with indo-1-AM (5μg/ml), and activated with anti-IgM (10μg/ml). The graph shows the ratio of bound to unbound indo-1-AM as a measure of Ca^{2+} influx. (D) Normal tyrosine phosphorylation in anti-IgM-stimulated *Usp8*$^{f/f}$*Cd19*-Cre B cells. Splenic B cells were purified, stimulated as in (B), and analyzed by WB. (E, F) Normal JNK activation and Ca^{2+} influx in *Usp8*$^{f/f}$*Rosa26*-CreERT2 splenic B cells upon short term USP8 depletion. (E) *Usp8*$^{f/f}$ and *Usp8*$^{f/f}$*Rosa26*-CreERT2 splenic B cells were expanded in medium containing IL-4 and CD40 for 24 h followed by OHT addition and further expansion for 48 h. Cells were stimulated as in (B). and lysates were subjected to WB analysis. Results are representative of at least two independent experiments. (F) Cells were expanded as in (E) for 72 h after OHT addition and Ca^{2+} influx was analyzed as in (C). (G) Pathway enrichment analysis on genes upregulated in B cell subsets of the indicated genotype.

Fig. S4. Role of K11- and K48-linked NEDD8 modifications in the formation of mixed ubiquitin/NEDD8 chains induced by catalytically inactive USP8. HEK293T cells were transfected with WT-USP8-FLAG or USP8(C786A)-FLAG in the presence of the indicated HA-NEDD8 variants and lysates were analyzed by WB. Results are representative of 2 independent experiments.

Fig. S5. Viability assay of BTZ resistant KMS-18-T21A MM cells upon treatment with 10nM (left panel) or 25 nM (right panel) BTZ in the presence of increasing DUB-IN-2 concentrations.

Fig. S6. (A) Pathway enrichment analysis of expression data from MM patients included in the analysis of the MMRF CoMMpass study. Patients were split into equal groups according to USP8 expression (< median and > median). (B) Lack of BM infiltration of KMS18 MM cells in NSG mice that had been treated with either control (0.9NaCl/PEG300 1:1 (v/v)), BTZ (0.6mg/kg), or BTZ combined with DUB-IN2 using 5mg/kg 5 times over a period of 13 days, followed by 2mg/kg twice a week.

Table S1. Antibodies/target-specific binding molecule list.

Experiment	**Marker/target-specific binding molecule**	**Clone ID**	**Source**
Histology	B220	RA3-6B2	BD Pharmingen
	CD3	CD3-12	Serotec
	IgD (biotinylated)	11.26.c.2a	BioLegend
	IgM	Polyclonal	Chemicon
	Moma1	MCA947	AbD Serotec
	Biotinylated peanut agglutinin (PNA)	# B-1075	Vector Laboratories
	Ki67	TEC-3	DAKO
FACS	Anti-CD16/CD32 (Fc Block™)	2.4G2	BD Pharmingen
	CD3ε	500A2	eBioscience

	CD19	MB19-1	eBioscience
	B220	RA3-6B2	BD Pharmingen
	IgD	11.26.c.2a	BD Pharmingen
	IgM	II/41	eBioscience
	CD5	53-7.3	BD Pharmingen
	CD21	7G6	BD Pharmingen
	CD23	B3B4	BD Pharmingen
	CD43	S7	BD Pharmingen
	CD93	AA4.1	eBioscience
	Ki67	B56	BD Pharmingen
	T- and B-cell activation antigen	GL7	BD Pharmingen
	Fas	Jo2	BD Pharmingen
	T- and B-cell activation antigen	GL7	BD Pharmingen
	CD138	281-2	BioLegend
	IRF4	REA201	Milteny
	IgG1	RMG1-1	BioLegend
	Blimp1	5E7	BioLegend
	IgM	RMM-1	BioLegend
	CD16/32	93	BioLegend
	CD19	6D5	BioLegend
	CD21/CD35	(CR2/CR1)	BioLegend
	CD25	3C7	BioLegend

	CD3	17A2	BioLegend
	CD335	29A1.4	BioLegend
	CD4	GK1.5	BD Pharmingen
	CD44	IM7	BioLegend
	CD62L	MEL-14	BioLegend
	CD8a	53-6.7	BioLegend
	F4/80	BM8	BioLegend
	FOXP3	150D	BioLegend
	I-A/I-E	M5/114.15.2	BioLegend
	IgM	RMM-1	BioLegend
	Ly-6C	HK1.4	BioLegend
	Ly6G	1A8	BD Pharmingen
	TCRbeta	H57-597	BioLegend
Western	USP8(13aa)	Polyclonal	[36]
	USP8 (X39)	Polyclonal	[77]
	α,β,γ Actin	I-19	Santa Cruz Biotechnology
	FLAG	M2	Sigma
	HA	3F10	Roche
	Ubiquitin	P4D1	Santa Cruz Biotechnology
	NEDD8	Polyclonal, #2745	Cell Signaling Technology
	NEDD8		Abcam
	phospho-p44/42	197G2	Cell Signaling Technology
	phospho-JNK	81E11	Cell Signaling Technology

	phospho-p38	3D7	Cell Signaling Technology
	phospho-Akt	Polyclonal, #9271	Cell Signaling Technology
	phospho-IκBα	14D4	Cell Signaling Technology
	Roquin1/2	3F12	[35]
	IκBα	Polyclonal, #9242	Cell Signaling Technology
	phosphotyrosine	PY20	BD Biosciences
	DR5	E9D7D	Cell Signaling Technology
	CHOP	L63F7	Cell Signaling Technology
	LC3A/B	Polyclonal, #4108	Cell Signaling Technology
	Caspase3	Polyclonal, #9662	Cell Signaling Technology
	Caspase8	D35G2	Cell Signaling Technology
	Caspase9	C9	Cell Signaling Technology
	XBP1s	E9V3E	Cell Signaling Technology

References

1. Robak, P. & Robak, T. Bortezomib for the Treatment of Hematologic Malignancies: 15 Years Later. *Drugs in R&D* **19**, 73–92 (2019).
2. Clague, M. J., Urbé, S. & Komander, D. Breaking the chains: deubiquitylating enzyme specificity begets function. *Nature Reviews Molecular Cell Biology* **20**, 338–352 (2019).
3. Dufner, A. & Knobeloch, K.-P. Ubiquitin-specific protease 8 (USP8/UBPy): a prototypic multidomain deubiquitinating enzyme with pleiotropic functions. *Biochem Soc Trans* **47**, 1867–1879 (2019).
4. Mizuno, E., Kitamura, N. & Komada, M. 14-3-3-dependent inhibition of the deubiquitinating activity of UBPY and its cancellation in the M phase. *Experimental Cell Research* **313**, 3624–3634 (2007).
5. Kakihara, K. *et al.* Molecular basis of ubiquitin-specific protease 8 autoinhibition by the WW-like domain. *Commun Biol* **4**, 1272 (2021).
6. Reincke, M. *et al.* Mutations in the deubiquitinase gene USP8 cause Cushing's disease. *Nature Genetics* **47**, 31 (2014).
7. Ma, Z.-Y. *et al.* Recurrent gain-of-function USP8 mutations in Cushing's disease. *Cell Res* **25**, 306–317 (2015).
8. Santelices, J., Ou, M., Maegawa, G. H. B., Hercik, K. & Edelmann, M. J. USP8 inhibition regulates autophagy flux and controls Salmonella infection. *Front Cell Infect Microbiol* **13**, 1070271 (2023).
9. Mauri, S. *et al.* USP8 Down-Regulation Promotes Parkin-Independent Mitophagy in the Drosophila Brain and in Human Neurons. *Cells* **12**, (2023).

10. Xiong, W. *et al.* USP8 inhibition reshapes an inflamed tumor microenvironment that potentiates the immunotherapy. *Nat Commun* **13**, 1700 (2022).
11. Yang, H. *et al.* Targeting ubiquitin-specific protease 8 sensitizes anti-programmed death-ligand 1 immunotherapy of pancreatic cancer. *Cell Death Differ* **30**, 560–575 (2023).
12. Xie, F. *et al.* USP8 promotes cancer progression and extracellular vesicle-mediated CD8+ T cell exhaustion by deubiquitinating the TGF-β receptor TβRII. *EMBO J* **41**, e108791 (2022).
13. Islam, M. T., Chen, F. & Chen, H. The oncogenic role of ubiquitin specific peptidase (USP8) and its signaling pathways targeting for cancer therapeutics. *Arch Biochem Biophys* **701**, 108811 (2021).
14. Enchev, R. I., Schulman, B. A. & Peter, M. Protein neddylation: beyond cullin-RING ligases. *Nat Rev Mol Cell Biol* **16**, 30–44 (2015).
15. Kim, W. *et al.* Systematic and quantitative assessment of the ubiquitin-modified proteome. *Mol Cell* **44**, 325–340 (2011).
16. Hjerpe, R. *et al.* Changes in the ratio of free NEDD8 to ubiquitin triggers NEDDylation by ubiquitin enzymes. *Biochem J* **441**, 927–936 (2012).
17. Hjerpe, R., Thomas, Y. & Kurz, T. NEDD8 Overexpression Results in Neddylation of Ubiquitin Substrates by the Ubiquitin Pathway. *Journal of Molecular Biology* **421**, 27–29 (2012).
18. Leidecker, O., Matic, I., Mahata, B., Pion, E. & Xirodimas, D. P. The ubiquitin E1 enzyme Ube1 mediates NEDD8 activation under diverse stress conditions. *Cell Cycle* **11**, 1142–1150 (2012).
19. Lobato-Gil, S. *et al.* Proteome-wide identification of NEDD8 modification sites reveals distinct proteomes for canonical and atypical NEDDylation. *Cell Reports* **34**, 108635 (2021).

20. Maghames, C. M. *et al.* NEDDylation promotes nuclear protein aggregation and protects the Ubiquitin Proteasome System upon proteotoxic stress. *Nat Commun* **9**, 4376–4376 (2018).
21. Kim, S. *et al.* Stress-induced NEDDylation promotes cytosolic protein aggregation through HDAC6 in a p62-dependent manner. *iScience* **24**, 102146 (2021).
22. Dufner, A. *et al.* The ubiquitin-specific protease USP8 is critical for the development and homeostasis of T cells. *Nature Immunology* **16**, 950 (2015).
23. Tey, P. Y. *et al.* Rapid turnover of CTLA4 is associated with a complex architecture of reversible ubiquitylation. *bioRxiv : the preprint server for biology* 2023.12.31.573735 Preprint at https://doi.org/10.1101/2023.12.31.573735 (2024).
24. Adoro, S. *et al.* Post-translational control of T cell development by the ESCRT protein CHMP5. *Nature Immunology* **18**, 780 (2017).
25. Zhang, T. *et al.* The role of ubiquitinase in B cell development and function. *Journal of Leukocyte Biology* **n/a**, (2020).
26. Satpathy, S. *et al.* Systems-wide analysis of BCR signalosomes and downstream phosphorylation and ubiquitylation. *Molecular Systems Biology* **11**, 810 (2015).
27. Tiedemann, R. E. *et al.* Identification of Molecular Vulnerabilities in Human Multiple Myeloma Cells by RNA Interference Lethality Screening of the Druggable Genome. *Cancer Res* **72**, 757 (2012).
28. Colombo, M. *et al.* Synthesis and Biological Evaluation of 9-Oxo-9H-indeno[1,2-b]pyrazine-2,3-dicarbonitrile Analogues as Potential Inhibitors of Deubiquitinating Enzymes. *ChemMedChem* **5**, 552–558 (2010).
29. Hobeika, E. *et al.* Testing gene function early in the B cell lineage in mb1-cre mice. *Proc Natl Acad Sci U S A* **103**, 13789–13794 (2006).

30. Nguyen, H. T. T., Guevarra, R. B., Magez, S. & Radwanska, M. Single-cell transcriptome profiling and the use of AID deficient mice reveal that B cell activation combined with antibody class switch recombination and somatic hypermutation do not benefit the control of experimental trypanosomosis. *PLoS Pathog* **17**, e1010026 (2021).
31. Enders, A. *et al.* Zinc-finger protein ZFP318 is essential for expression of IgD, the alternatively spliced Igh product made by mature B lymphocytes. *Proc Natl Acad Sci U S A* **111**, 4513–4518 (2014).
32. Tellier, J. *et al.* Blimp-1 controls plasma cell function through the regulation of immunoglobulin secretion and the unfolded protein response. *Nat Immunol* **17**, 323–330 (2016).
33. Lee, S. K. *et al.* Interferon-γ Excess Leads to Pathogenic Accumulation of Follicular Helper T Cells and Germinal Centers. *Immunity* **37**, 880–892 (2012).
34. Raj, T., Negraschus, A. & Heissmeyer, V. Roquin-dependent gene regulation in immune-mediated diseases and future therapies. *Int Immunol* **35**, 159–170 (2023).
35. Vogel, K. U. *et al.* Roquin Paralogs 1 and 2 Redundantly Repress the Icos and Ox40 Costimulator mRNAs and Control Follicular Helper T Cell Differentiation. *Immunity* **38**, 655–668 (2013).
36. Niendorf, S. *et al.* Essential Role of Ubiquitin-Specific Protease 8 for Receptor Tyrosine Kinase Stability and Endocytic Trafficking In Vivo. *Mol. Cell. Biol.* **27**, 5029 (2007).
37. Row, P. E., Prior, I. A., McCullough, J., Clague, M. J. & Urbé, S. The Ubiquitin Isopeptidase UBPY Regulates Endosomal Ubiquitin Dynamics and Is Essential for Receptor Down-regulation. *Journal of Biological Chemistry* **281**, 12618–12624 (2006).
38. Pelzer, C. *et al.* The protease activity of the paracaspase MALT1 is controlled by monoubiquitination. *Nature Immunology* **14**, 337–345 (2013).

39. Schairer, R. *et al.* Allosteric activation of MALT1 by its ubiquitin-binding Ig3 domain. *Proceedings of the National Academy of Sciences* **117**, 3093–3102 (2020).

40. Xu, G., Paige, J. S. & Jaffrey, S. R. Global analysis of lysine ubiquitination by ubiquitin remnant immunoaffinity profiling. *Nat Biotechnol* **28**, 868–873 (2010).

41. Morrow, M. E. *et al.* Active site alanine mutations convert deubiquitinases into high-affinity ubiquitin-binding proteins. *EMBO Rep* **19**, e45680 (2018).

42. Sarparanta, J., Jonson, P. H., Kawan, S. & Udd, B. Neuromuscular Diseases Due to Chaperone Mutations: A Review and Some New Results. *Int J Mol Sci* **21**, 1409 (2020).

43. Westhoff, B., Chapple, J. P., van der Spuy, J., Höhfeld, J. & Cheetham, M. E. HSJ1 Is a Neuronal Shuttling Factor for the Sorting of Chaperone Clients to the Proteasome. *Current Biology* **15**, 1058–1064 (2005).

44. Avvakumov, G. V. *et al.* Amino-terminal Dimerization, NRDP1-Rhodanese Interaction, and Inhibited Catalytic Domain Conformation of the Ubiquitin-specific Protease 8 (USP8). *Journal of Biological Chemistry* **281**, 38061–38070 (2006).

45. Ekkebus, R. *et al.* On Terminal Alkynes That Can React with Active-Site Cysteine Nucleophiles in Proteases. *J. Am. Chem. Soc.* **135**, 2867–2870 (2013).

46. Geurink, P. P. *et al.* Chapter Sixteen - Profiling DUBs and Ubl-specific proteases with activity-based probes. in *Methods in Enzymology* (ed. Hochstrasser, M.) vol. 618 357–387 (Academic Press, 2019).

47. Coleman, K. E. *et al.* SENP8 limits aberrant neddylation of NEDD8 pathway components to promote cullin-RING ubiquitin ligase function. *Elife* **6**, e24325 (2017).

48. Vogl, A. M. *et al.* Global site-specific neddylation profiling reveals that NEDDylated cofilin regulates actin dynamics. *Nature Structural & Molecular Biology* **27**, 210–220 (2020).

49. Impens, F., Radoshevich, L., Cossart, P. & Ribet, D. Mapping of SUMO sites and analysis of SUMOylation changes induced by external stimuli. *Proc Natl Acad Sci USA* **111**, 12432 (2014).

50. Brancolini, C. & Iuliano, L. Proteotoxic Stress and Cell Death in Cancer Cells. *Cancers (Basel)* **12**, (2020).

51. Allmeroth, K. *et al.* Bortezomib resistance mutations in PSMB5 determine response to second-generation proteasome inhibitors in multiple myeloma. *Leukemia* **35**, 887–892 (2021).

52. Brewer, J. W. Regulatory crosstalk within the mammalian unfolded protein response. *Cellular and Molecular Life Sciences* **71**, 1067–1079 (2014).

53. Xiong, S., Chng, W.-J. & Zhou, J. Crosstalk between endoplasmic reticulum stress and oxidative stress: a dynamic duo in multiple myeloma. *Cell Mol Life Sci* **78**, 3883–3906 (2021).

54. Chen, L. *et al.* Gefitinib enhances human colon cancer cells to TRAIL-induced apoptosis of via autophagy- and JNK-mediated death receptors upregulation. *Apoptosis* **21**, 1291–1301 (2016).

55. Dhanasekaran, D. N. & Reddy, E. P. JNK-signaling: A multiplexing hub in programmed cell death. *Genes Cancer* **8**, 682–694 (2017).

56. Voronina, M. V. *et al.* The Intricate Balance between Life and Death: ROS, Cathepsins, and Their Interplay in Cell Death and Autophagy. *Int J Mol Sci* **25**, (2024).

57. Di Yu *et al.* Roquin represses autoimmunity by limiting inducible T-cell co-stimulator messenger RNA. *Nature* **450**, 299–303 (2007).

58. Ramiscal, R. R. *et al.* Attenuation of AMPK signaling by ROQUIN promotes T follicular helper cell formation. *Elife* **4**, e08698 (2015).

59. Essig, K. *et al.* Roquin Suppresses the PI3K-mTOR Signaling Pathway to Inhibit T Helper Cell Differentiation and Conversion of Treg to Tfr Cells. *Immunity* **47**, 1067-1082.e12 (2017).

60. Bertossi, A. *et al.* Loss of Roquin induces early death and immune deregulation but not autoimmunity. *J Exp Med* **208**, 1749–1756 (2011).

61. Vinuesa, C. G. *et al.* A RING-type ubiquitin ligase family member required to repress follicular helper T cells and autoimmunity. *Nature* **435**, 452–458 (2005).

62. Chevrier, S., Kratina, T., Emslie, D., Karnowski, A. & Corcoran, L. M. Germinal center-independent, IgM-mediated autoimmunity in sanroque mice lacking Obf1. *Immunology & Cell Biology* **92**, 12–19 (2014).

63. Mori, F. *et al.* Accumulation of NEDD8 in neuronal and glial inclusions of neurodegenerative disorders. *Neuropathology and Applied Neurobiology* **31**, 53–61 (2005).

64. Dil Kuazi, A. *et al.* NEDD8 protein is involved in ubiquitinated inclusion bodies. *The Journal of Pathology* **199**, 259–266 (2003).

65. Alexopoulou, Z. *et al.* Deubiquitinase Usp8 regulates α-synuclein clearance and modifies its toxicity in Lewy body disease. *Proc Natl Acad Sci U S A* **113**, E4688–E4697 (2016).

66. von Stockum, S. *et al.* Inhibition of the deubiquitinase USP8 corrects a Drosophila PINK1 model of mitochondria dysfunction. *Life Sci Alliance* **2**, e201900392 (2019).

67. Rickert, R. C., Roes, J. & Rajewsky, K. B lymphocyte-specific, Cre-mediated mutagenesis in mice. *Nucleic Acids Res* **25**, 1317–1318 (1997).

68. Hameyer, D. *et al.* Toxicity of ligand-dependent Cre recombinases and generation of a conditional Cre deleter mouse allowing mosaic recombination in peripheral tissues. *Physiological Genomics* **31**, 32–41 (2007).

69. Shultz, L. D. *et al.* Human lymphoid and myeloid cell development in NOD/LtSz-scid IL2R gamma null mice engrafted with mobilized human hemopoietic stem cells. *J Immunol* **174**, 6477–6489 (2005).

70. Young, M. D. & Behjati, S. SoupX removes ambient RNA contamination from droplet-based single-cell RNA sequencing data. *GigaScience* **9**, giaa151 (2020).

71. Linderman, G. C. *et al.* Zero-preserving imputation of single-cell RNA-seq data. *Nature Communications* **13**, 192 (2022).

72. Kim, K. J., Kanellopoulos-Langevin, C., Merwin, R. M., Sachs, D. H. & Asofsky, R. Establishment and Characterization of BALB/c Lymphoma Lines with B Cell Properties. *J. Immunol.* **122**, 549 (1979).

73. Justement, L. B., Wienands, J., Hombach, J., Reth, M. & Cambier, J. C. Membrane IgM and IgD molecules fail to transduce Ca2+ mobilizing signals when expressed on differentiated B lineage cells. *J. Immunol.* **144**, 3272 (1990).

74. Blank, T. *et al.* Brain Endothelial- and Epithelial-Specific Interferon Receptor Chain 1 Drives Virus-Induced Sickness Behavior and Cognitive Impairment. *Immunity* **44**, 901–912 (2016).

75. El Oualid, F. *et al.* Chemical synthesis of ubiquitin, ubiquitin-based probes, and diubiquitin. *Angew Chem Int Ed Engl* **49**, 10149–10153 (2010).

76. Colaprico, A. *et al.* TCGAbiolinks: an R/Bioconductor package for integrative analysis of TCGA data. *Nucleic Acids Res* **44**, e71 (2016).

77. Gnesutta, N. *et al.* Cloning and Characterization of Mouse UBPy, a Deubiquitinating Enzyme That Interacts with the Ras Guanine Nucleotide Exchange Factor CDC25Mm/Ras-GRF1. *Journal of Biological Chemistry* **276**, 39448–39454 (2001).

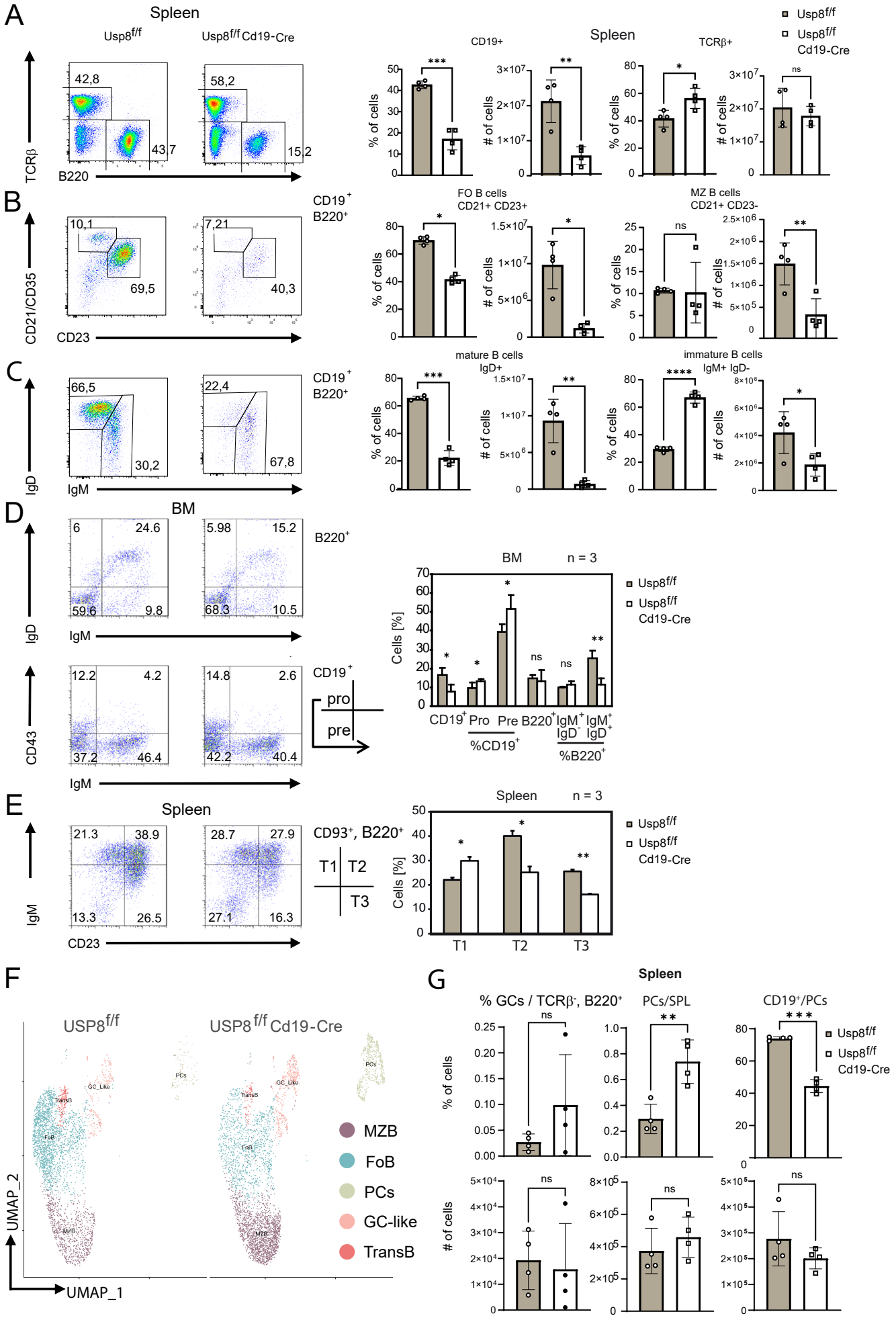

Dufner et al., Figure 1

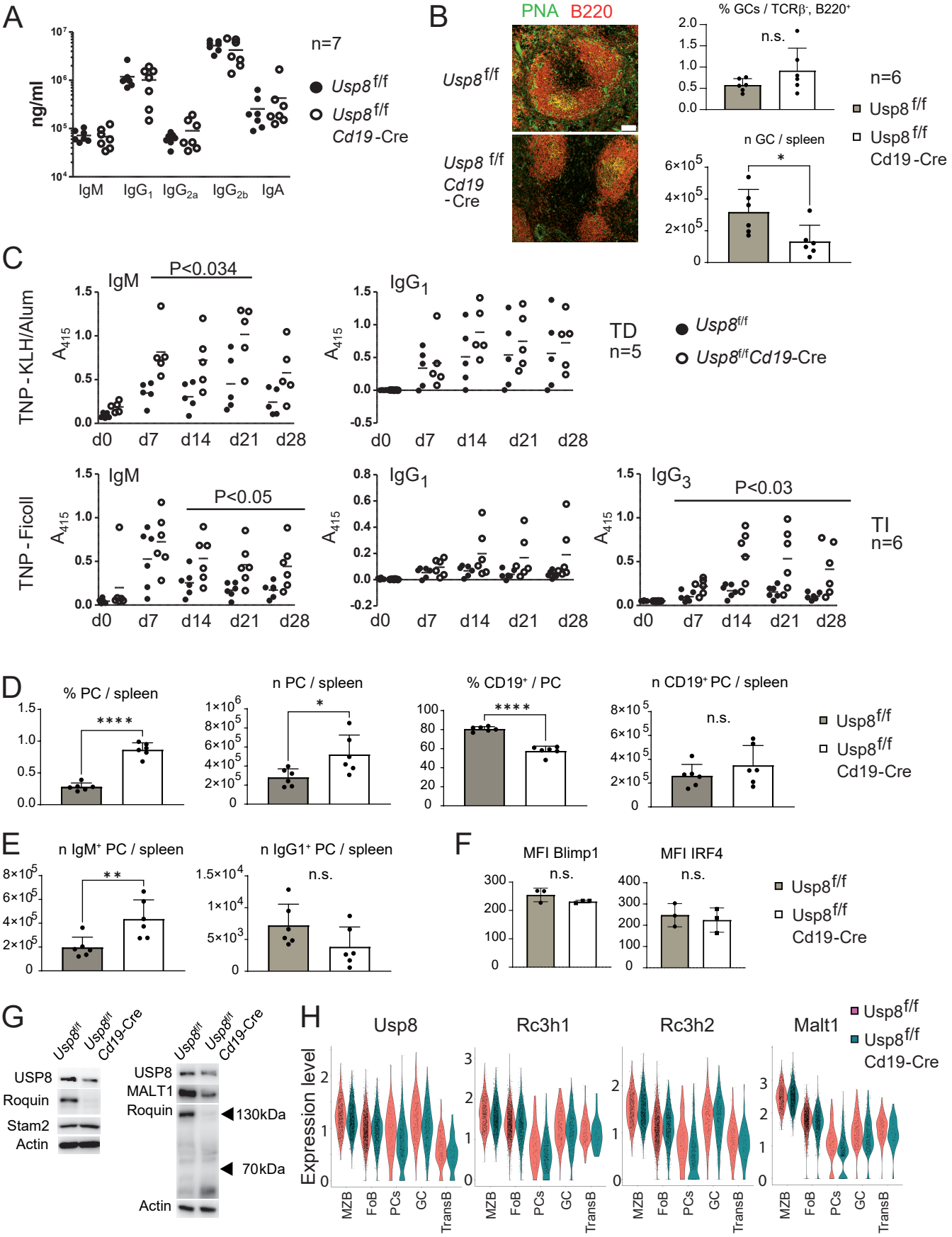

Dufner et al., Figure 2

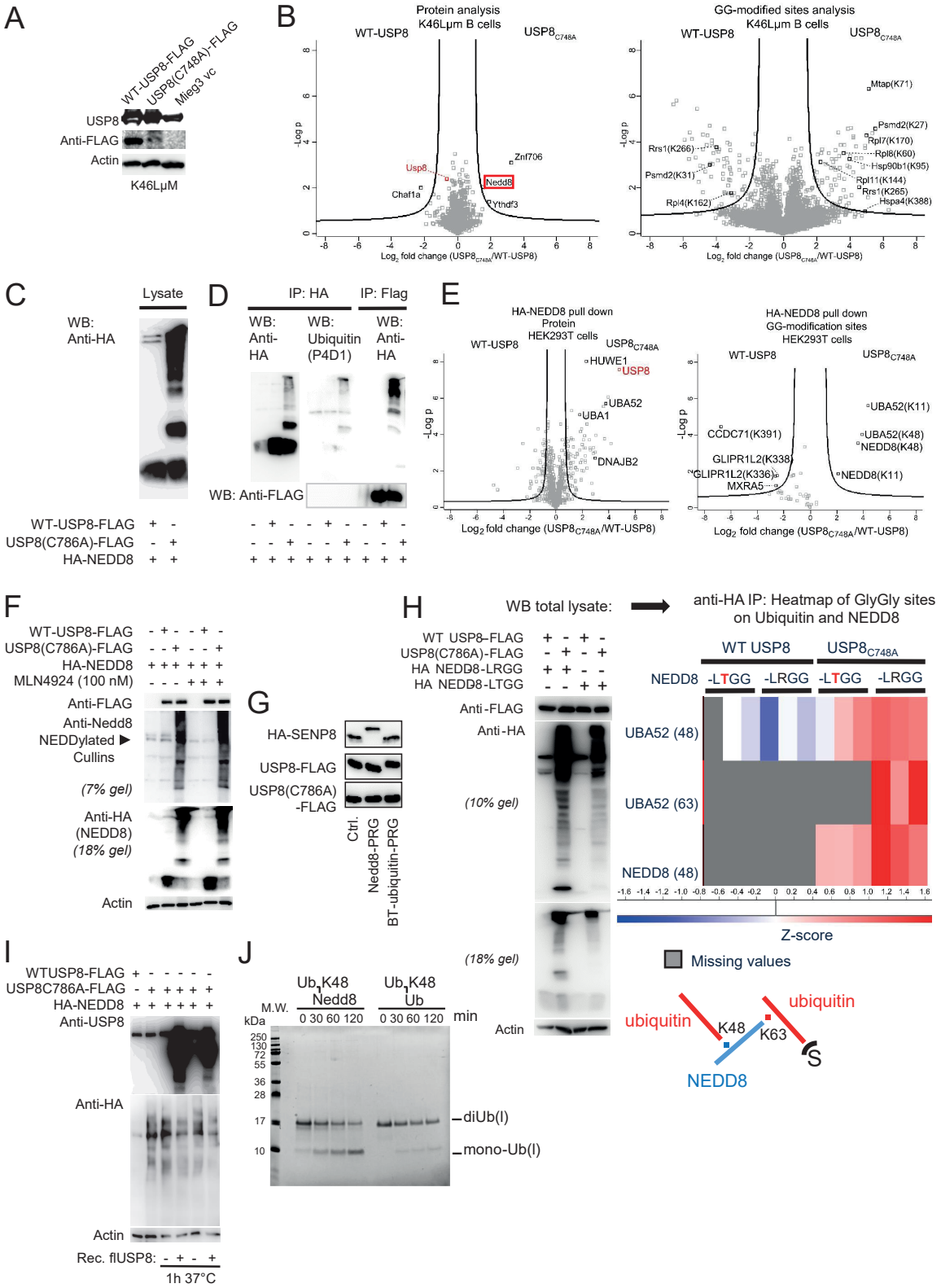

Dufner et al., Figure 3

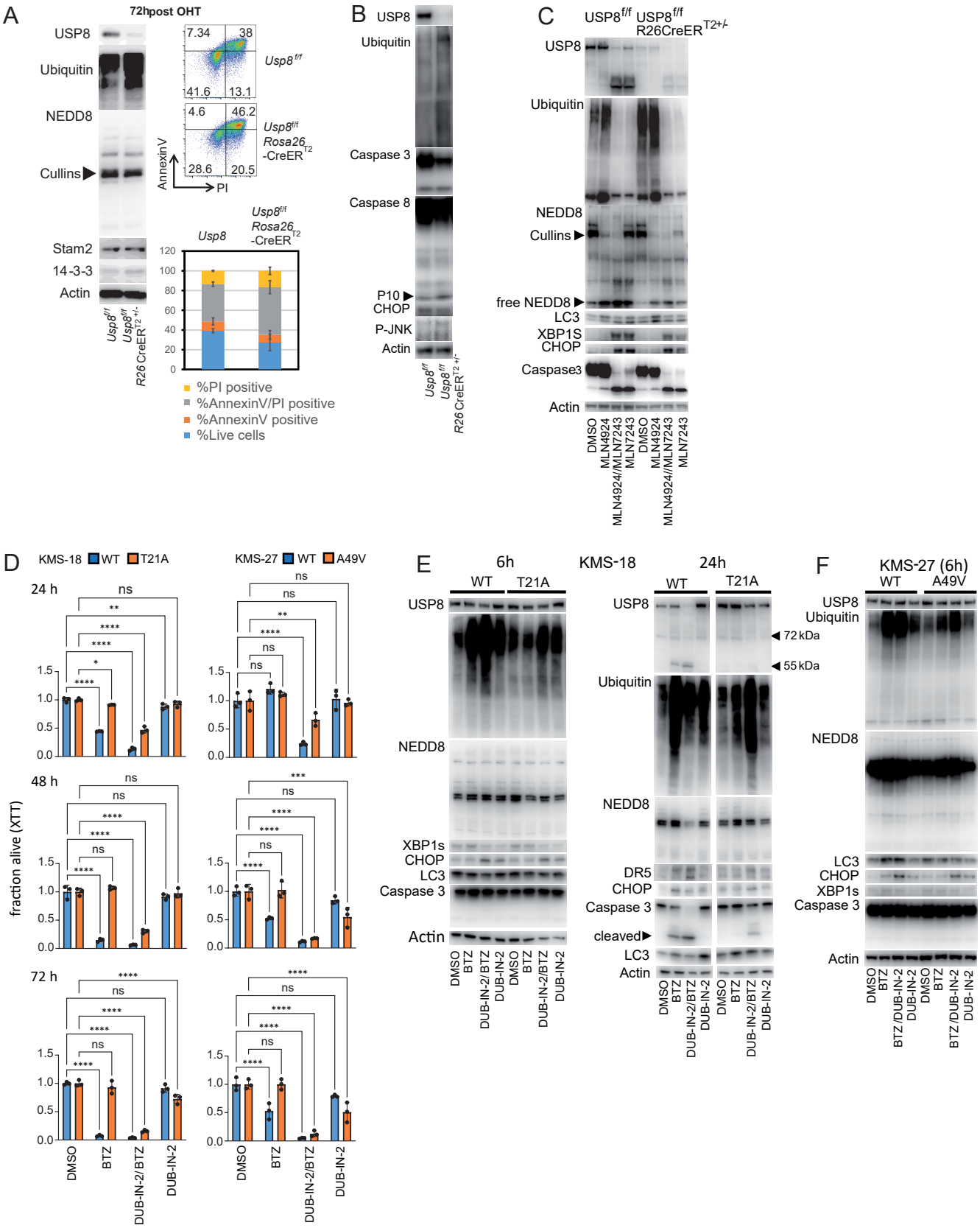

Dufner et al., Figure 4

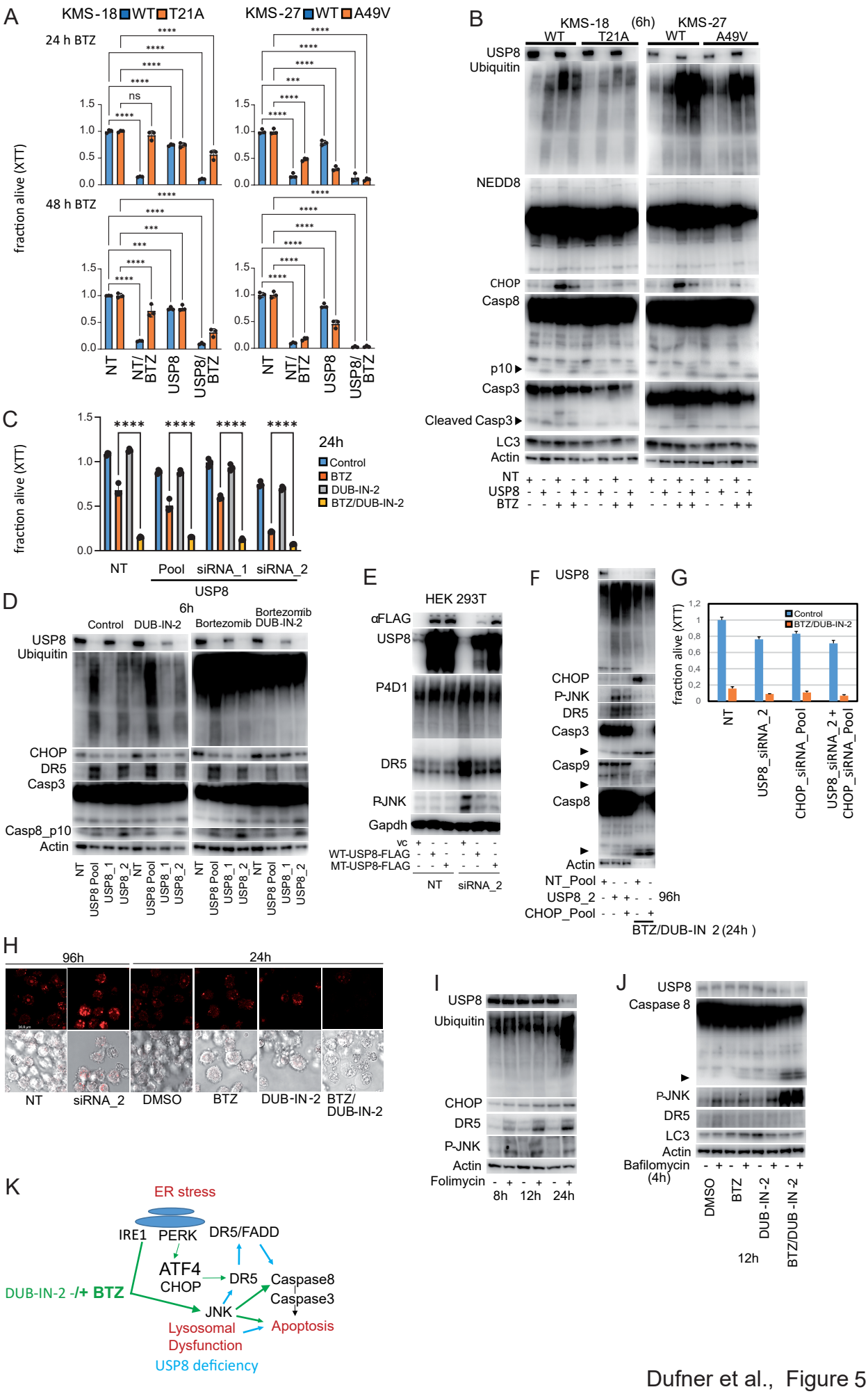

Dufner et al., Figure 5

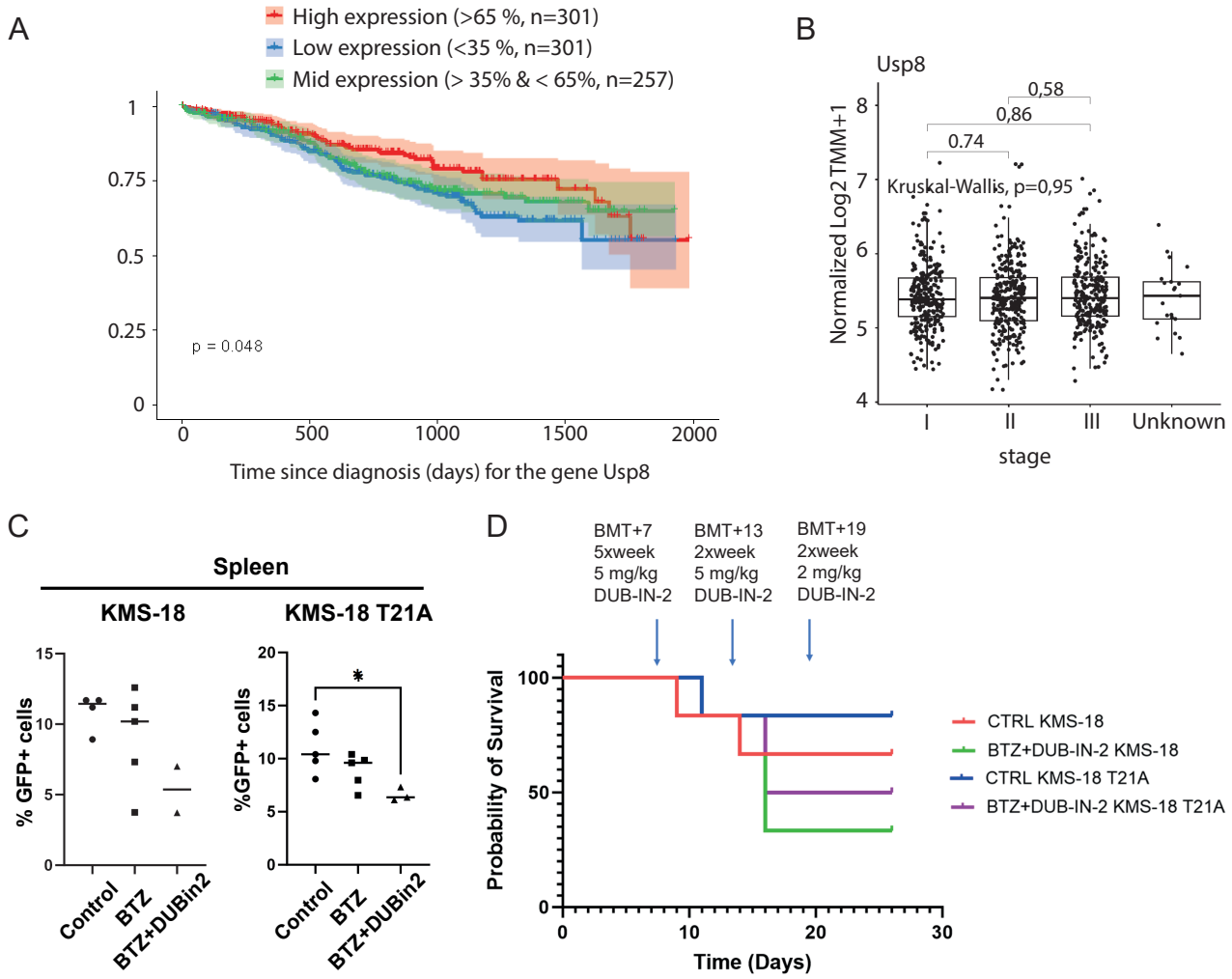

Dufner et al., Fig. 6

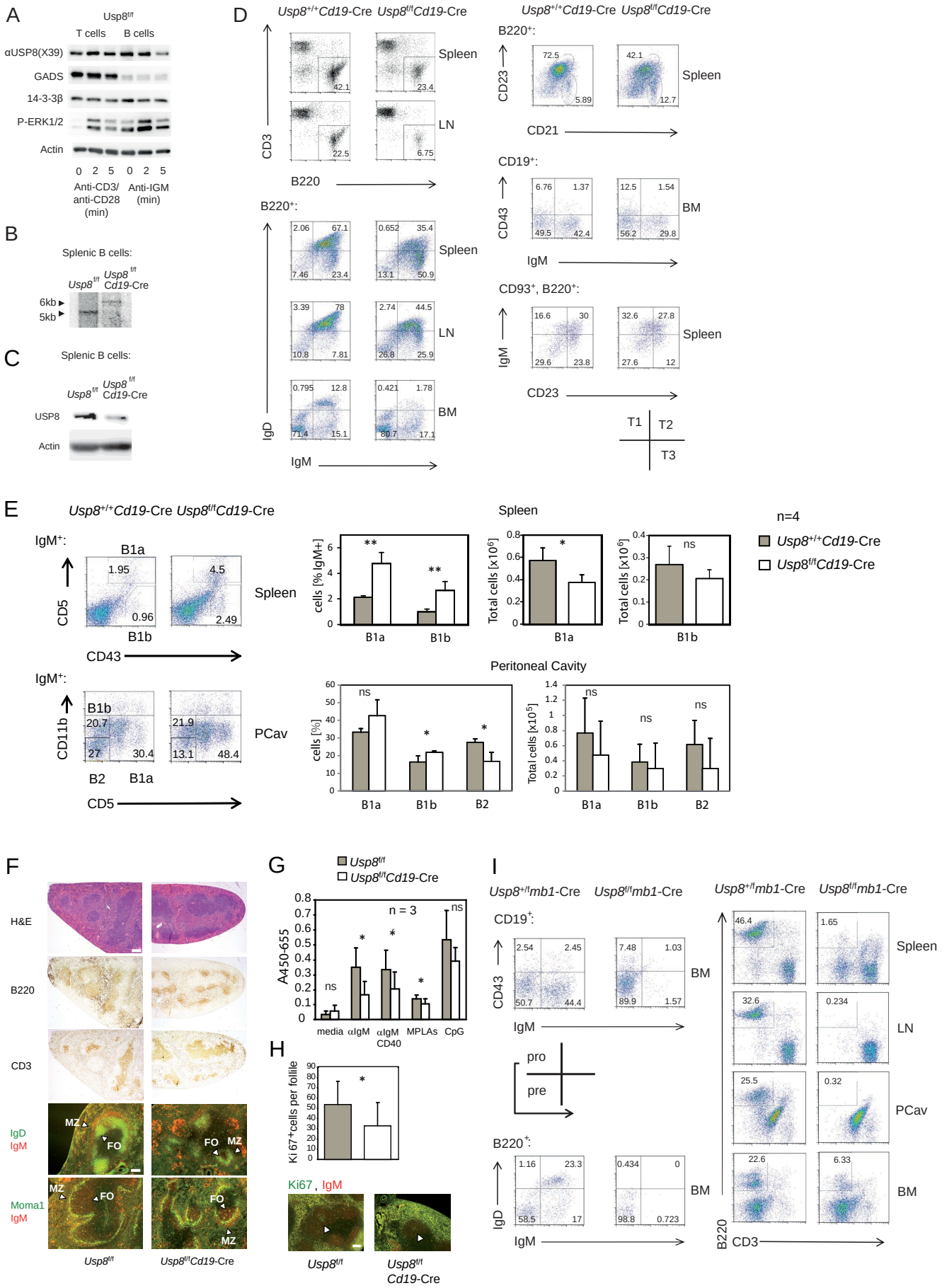

Dufner et al., Figure S1

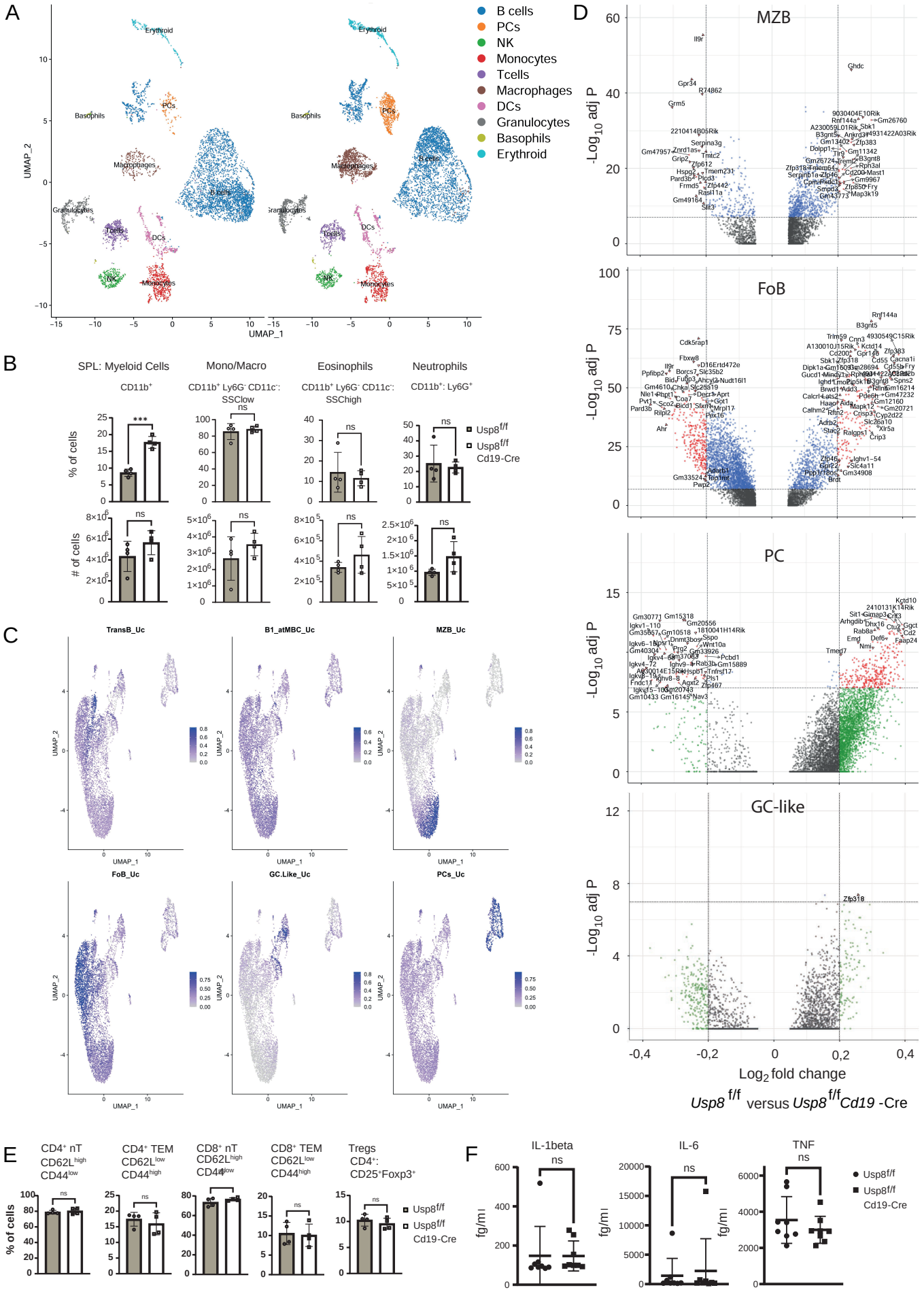

Dufner et al., Figure S2

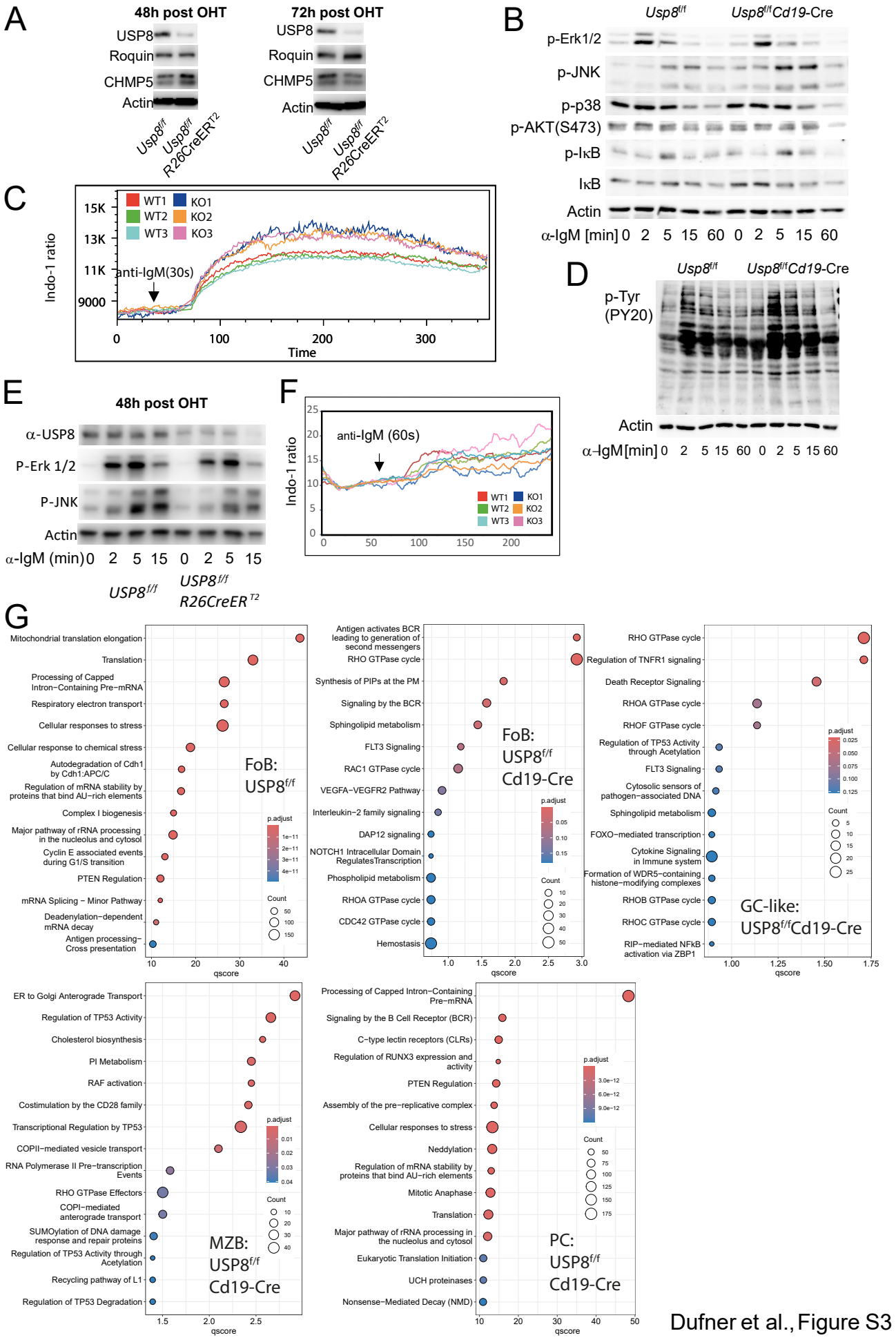

Dufner et al., Figure S3

A

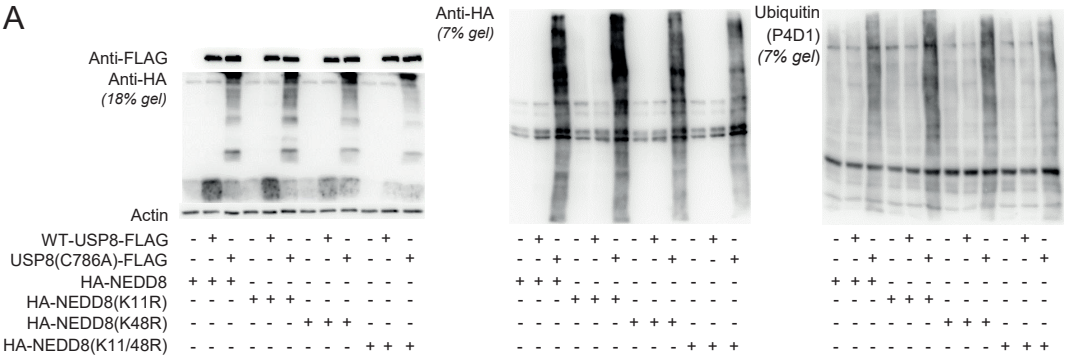

Dufner et al., Figure S4

A

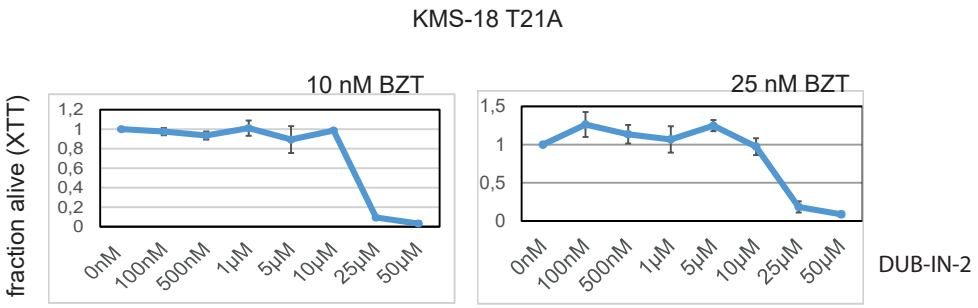

Dufner et al., Figure S5

A

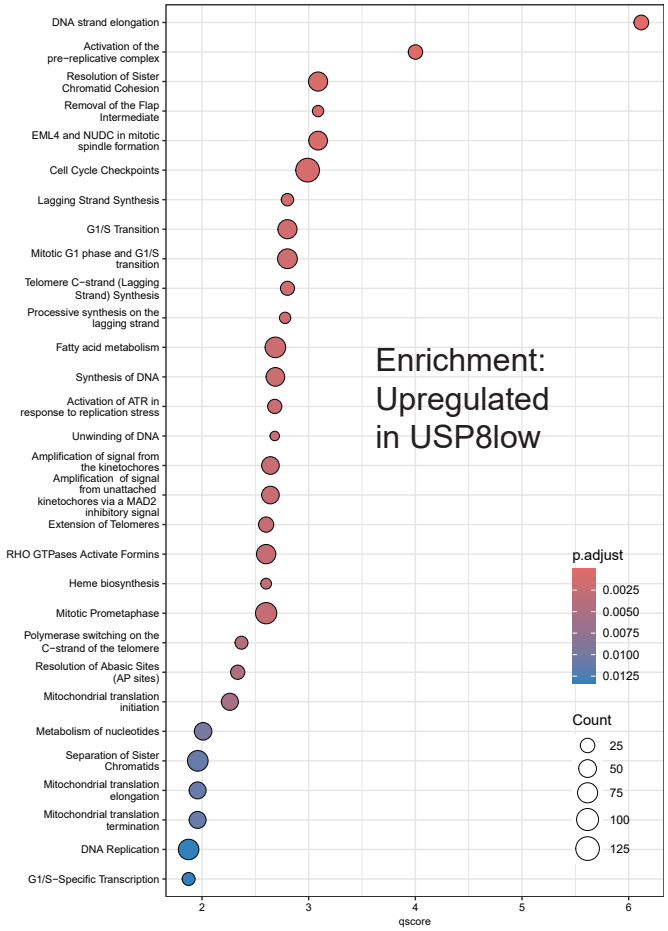

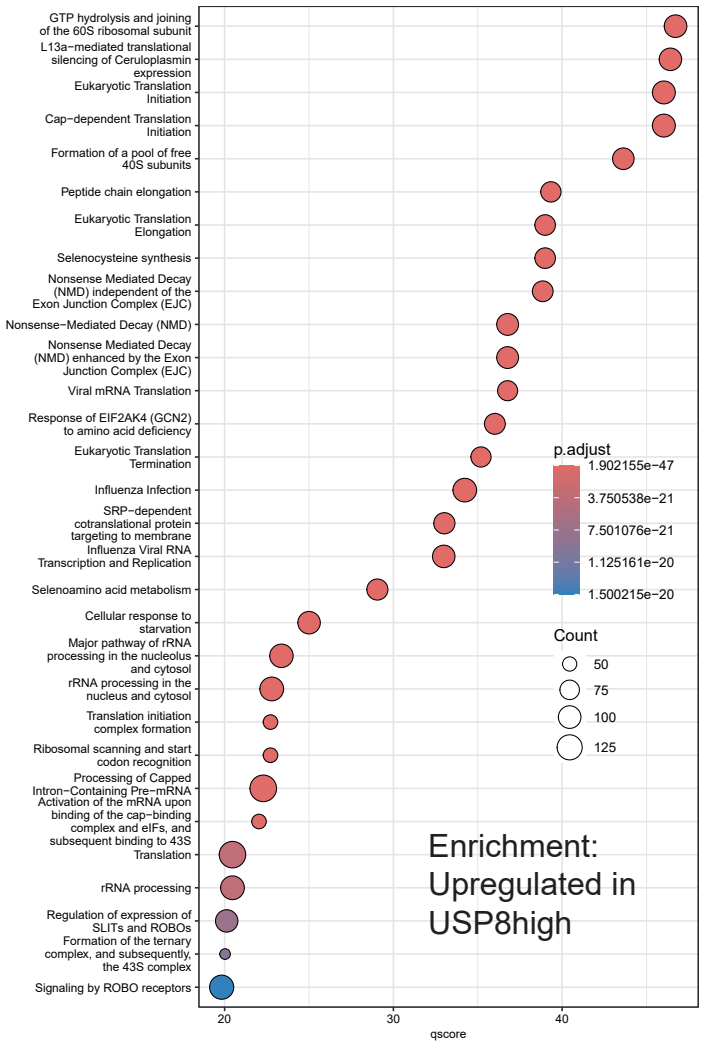

B

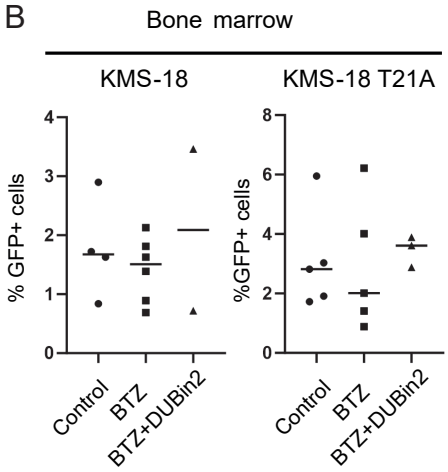

Dufner et al., Fig. S6